Tennessee State University

Digital Scholarship @ Tennessee State University

New Precision Orbits of Bright Double-Lined Spectroscopic Binaries. VIII. HR 1528, HR 6993, 2 Sagittae, and 18 Vulpeculae

Francis C. Fekel
Tennessee State University

Jocelyn Tomkin
University of Texas at Austin

Michael H. Williamson
Tennessee State University

Recommended Citation

NEW PRECISION ORBITS OF BRIGHT DOUBLE-LINED SPECTROSCOPIC BINARIES. VIII. HR 1528, HR 6993, 2 SAGITTAE, AND 18 VULPECULAE

FRANCIS C. FEKEL[1,3], JOCELYN TOMKIN[2], AND MICHAEL H. WILLIAMSON[1]

[1] Center of Excellence in Information Systems, Tennessee State University, 3500 John A. Merritt Boulevard,
Box 9501, Nashville, TN 37209, USA; fekel@evans.tsuniv.edu, michael.h.williamson@gmail.com
[2] Astronomy Department and McDonald Observatory, University of Texas, Austin, TX 78712, USA; jt@alexis.as.utexas.edu

ABSTRACT

Improved orbital elements for four A-star double-lined spectroscopic binaries have been determined with numerous new radial velocities. Three of the four systems, HR 1528, 2 Sge, and 18 Vul, have moderately short orbital periods of 7.05, 7.39, and 9.31 days, respectively, and also have circular or nearly circular orbits. Only HR 6993 with a period of 14.68 days has a significantly eccentric orbit. The close visual companion of 2 Sge has been detected spectroscopically, and its velocity measured. The orbital dimensions ($a_1 \sin i$ and $a_2 \sin i$) and minimum masses ($m_1 \sin^3 i$ and $m_2 \sin^3 i$) of the short-period binary components all have accuracies of 0.5% or better. We determine basic properties of the individual stars and compare them with solar-abundance evolutionary tracks to estimate their masses. Half of the eight components may be synchronously or pseudosynchronously rotating.

Key words: binaries: spectroscopic – stars: fundamental parameters – stars: individual
(HR 1528, HR 6993, 2 Sge, 18 Vul)

1. INTRODUCTION

With the advances in ground-based optical and near-infrared interferometry over the past decades, there is now a greatly enhanced overlap of the spectroscopic and visual binary domains (Quirrenbach 2001). This has resulted in a significant increase in the number of binary stars that can be resolved with both spectroscopy and astrometry, expanding the possibilities for the direct determination of stellar masses and precise stellar parallaxes from their three-dimensional orbits. There are now more than 30 interferometric visual orbits for systems containing double-lined spectroscopic binaries (Cunha et al. 2007) and at least 23 interferometric binaries that have masses determined to an accuracy of 3% or better (Torres et al. 2010). The determination of three-dimensional orbits and precise masses (e.g., Hummel et al. 2001; Boden et al. 2006; Fekel et al. 2009a) has resulted in valuable comparisons with stellar evolutionary theory.

In the current edition of the spectroscopic binary orbit catalog, SB9 (Pourbaix et al. 2004), there are still many stars with orbits that have been determined with photographic plate velocities. Such velocities are much less precise than those from modern CCD observations and thus would significantly limit the precision of combined spectroscopic–astrometric orbits. In our series of orbit papers (Tomkin & Fekel 2006, 2008; Fekel et al. 2009b, 2010, 2011a, 2011b; Fekel & Williamson 2010), we have acquired new radial velocities from three observatories and used them to redetermine the orbits for 19 bright spectroscopic binaries. Interferometric observations of those systems will lead to three-dimensional orbits and well-determined masses and parallaxes. Some basic information about the four A-star double-lined binaries that are analyzed in this paper is given in Table 1.

2. BRIEF HISTORY

2.1. HR 1528 = HD 30453 = HIP 22407

Harper (1932a) discovered HR 1528 [$\alpha = 04^h49^m19^s08$, $\delta = 32°35'17''.5$ (2000)] to be a single-lined spectroscopic binary with a period of 7.0507 days and a near circular orbit. Using Harper's data, Luyten (1936) derived similar elements, while Lucy & Sweeney (1971) concluded that the orbit was circular. As shown in their Figure 8, Stockton & Fekel (1992) detected lines of the secondary at red wavelengths. They included Harper's data to improve the period and then computed a circular orbit for the double-lined spectroscopic binary. In 1984, McAlister et al. (1987), using speckle interferometry, announced the discovery of a third component with a separation of 0''.04.

HR 1528 is a well-known metallic-lined star. Appenzeller (1967) gave it an A4m spectral classification, while Bertaud & Floquet (1967) provided a more detailed description, calling its Ca K line A7 and its metal lines F2. Cowley et al. (1969) classified the Ca K line as A8m. The most complete description of the Am star spectrum was provided by Abt & Morrell (1995), who assigned types of A7, F0, and F2 to the Ca K, hydrogen, and metal lines, respectively. The star is slowly rotating with $v \sin i$ values of 15 km s^{-1} (Abt & Moyd 1973; Abt & Morrell 1995) and 10 km s^{-1} (Stockton & Fekel 1992).

2.2. HR 6993 = HD 171978 = HIP 91322

Adams (1915) first reported the radial velocity of HR 6993 [$\alpha = 18^h37^m35^s96$, $\delta = -00°18'34''.1$ (2000)] but did not note any variability. Several decades later Petrie (1948) surveyed stars that were believed to be members of the Ursa Major moving group and immediately discovered its duplicity. Collecting additional high-dispersion observations, he determined an orbit with a period of 14.674 days and an eccentricity of 0.211 for this double-lined early-type spectroscopic binary.

Cowley et al. (1969) and Floquet (1975) classified HR 6993 as A2 V, while Levato & Abt (1978) concurred in that classification but also noted that the lines were sharp. Geary & Abt (1970) concluded that the secondary component appears to be an Am

Table 1
Basic Properties of the Program Stars

Name	HR	HD	Spectral Type	V^a (mag)	$B - V^a$ (mag)	Parallax^b (mas)	Period (days)
. . .	1528	30453	Am	5.84	0.250	11.94	7.05
. . .	6993	171978	A2 V	5.76	0.067	6.23	14.68
2 Sge	7369	182490	A1 III	6.27	0.075	8.92	7.39
18 Vul	7711	191747	A2 IV	5.51	0.087	7.70	9.31

Notes.
^{a} Perryman et al. (1997).
^{b} van Leeuwen (2007).

star. Petrie (1948) stated that both components had sharp lines, a result that was quantified by Geary & Abt (1970), who determined $v \sin i$ values of <10 km s^{-1} for both components. A larger value of 35 km s^{-1}, found by Abt & Morrell (1995), appears to be from an orbital phase when the lines are partially blended.

2.3. 2 Sge = HR 7369 = HD 182490 = HIP 109647

From the measurement of two Mount Wilson Observatory plates, Adams (1912) announced the velocity variability of 2 Sge [$\alpha = 19^h24^m22^s07$, $\delta = 16°56'15''8$ (2000)]. Following up on that discovery, at the Dominion Observatory of Ottawa, Young (1917) acquired 44 observations with a one-prism spectrograph, and some of those spectrograms showed lines of the secondary. Using velocities from those plates as well as values from the two discovery observations, Young (1917) determined an initial orbital solution, which he characterized as a first approximation, that resulted in a nearly circular orbit with a period of 7.390 days. Lines of the secondary were so difficult to measure that they were only used to determine the semi-amplitude of the secondary. Young (1917) mentioned that the spectral lines of 2 Sge are fairly sharp and narrow. In his reexamination of 64 orbits, Harper (1935) used six spectra of 2 Sge, obtained at the Dominion Astrophysical Observatory (DAO), to revise the orbital period to 7.3919 days. The binary was one of 77 systems with small orbital eccentricities that Luyten (1936) reanalyzed. Using the 44 Dominion Observatory observations only, he adopted a circular orbit and recomputed the elements.

Analysis of the *Hipparcos* data resulted in the discovery of a faint, close visual companion to 2 Sge (Perryman et al. 1997). Fabricius & Makarov (2000) determined a *Tycho V*-band difference of 3.8 mag, while Roberts (2011) measured a Bessel *I*-band difference of 3.4 mag. Mason et al. (1999) followed up the discovery observation with a very weak ground-based detection in 1996. More recently, Roberts (2011) resolved the components again, showing that the pair were still separated by 0.''4 but had rotated 11° in 11 yr.

Over the years, a number of different spectral types have been assigned to 2 Sge. Osawa (1959) classified 2 Sge as A2 III? and noted that its metal lines had an A3 class. Cowley et al. (1969) called the Ca K line A1 and stated that the star's metal lines were marginally enhanced, indicating that 2 Sge is a mild metallic-lined A star. Bidelman (Abt & Bidelman 1969) concluded that it is a probable Am star, while Bertaud (1970) classified it as a full-fledged Am star with its Ca K line being A2 and its metal lines A7. Other classifiers have found no spectrum peculiarities. Levato (1975) assigned a spectral type of A2 III–IV, while Abt & Morrell (1995) classified its spectral type as A1 III. In addition, Cucchiaro et al. (1978) obtained an ultraviolet spectrum of 2 Sge with the sky survey telescope of

the *TD1* satellite and classified the star as an A2 giant. Stickland (1973) performed a spectroscopic abundance analysis of both components and concluded that Fe was overabundant in both stars. Using four Fe I line pairs in the blue region of the spectrum, Petrie (1950) estimated a magnitude difference of 0.65 for the short-period binary. Levato (1975) determined a $v \sin i$ value of 50 km s^{-1}, while Abt & Morrell (1995) found a smaller value of 35 km s^{-1}.

2.4. 18 Vul = HR 7711 = HD 191747 = HIP 99404

Velocity measurements of three spectroscopic plates, obtained at Mount Wilson Observatory, led Adams (1915) to announce the binary nature of 18 Vul [$\alpha = 20^h10^m33^s54$, $\delta = 26°54'15''0$ (2000)] with the components having a velocity separation of 150 km s^{-1} on one plate. Following up on this discovery, Harper (1918) collected 62 usable spectra at the Dominion Observatory at Ottawa from which he computed a nearly circular orbit with a period of 9.316 days. With the acquisition of five additional velocities, he later decreased the period to 9.314 days (Harper 1935). Luyten (1936) reanalyzed the velocities and considered the orbit to be circular.

Osawa (1959) gave a spectral type of A3 III for the combined system. That result was followed by Svolopoulos (1961), who classified a number of stars in open clusters and included 18 Vul as A1 IV. Additional spectral types of A3 V (Cowley et al. 1969) and A2 IV (Abt & Morrell 1995) have been given. Cucchiaro et al. (1978) examined an ultraviolet spectrum of 18 Vul with the sky survey telescope of the *TD1* satellite and classified the star as an A3 dwarf from ultraviolet criteria. Bidelman (Abt & Bidelman 1969) concluded that its spectrum was that of a normal A star with no peculiarities.

Breger (1969) included 18 Vul in a search for δ Scuti variables among more than 200 bright field stars. His limited observations indicated that the star was constant at a level of 2 mmag. However, later photometric observations by Belmonte & Roca Cortés (1989) revealed low-amplitude variability of 4 mmag with a period of 2.9 hr. Although classified as a δ Scuti variable, its position is somewhat blueward of the blue edge of the δ Scuti instability strip (Rodríguez et al. 1994).

3. OBSERVATIONS AND RADIAL VELOCITIES

We acquired spectroscopic observations of the four program stars at three different observatories. From 2002 through 2007, we collected spectra at McDonald Observatory with the 2.1 m telescope, the Sandiford Cassegrain echelle spectrograph (McCarthy et al. 1993), and a Reticon CCD. The wavelength range covered by those spectrograms is 5700–7000 Å and the resolving power is 49,000.

From 2004 through 2012, we also obtained spectrograms of the binaries at Kitt Peak National Observatory (KPNO) with the coudé feed telescope and coudé spectrograph. The vast majority of the observations were made with a Texas Instruments (TI) CCD detector. Those spectra are mostly centered at 6430 Å, cover a wavelength range of 84 Å, and have a resolution of 0.21 Å or a resolving power of just over 30,000. A few spectra were centered in the blue at 4500 Å but with the same wavelength range of 84 Å and resolution, producing a resolving power of 21,000. When the TI detector was unavailable in 2008 September, we used instead a Tektronics CCD, designated T1KA. With that CCD the spectrum was centered at 6400 Å, the wavelength coverage increased to 172 Å, and the resolving power decreased to 19,000. The TI CCD was retired from

service in 2010 September. As a result, our observations from that point forward were obtained with a new CCD, made by Semiconductor Technology Associates and given the designation STA2. It consists of a 2600×4000 array of $12\,\mu$m pixels. With STA2 the spectrum once again was centered at 6430 Å, and the size of the detector produced a wavelength range of 336 Å. The spectrograph slit was set so that the STA2 spectra have the same resolution as those acquired with the TI CCD although there is some worsening of the resolution at both ends of the STA2 spectra. Additional information about our McDonald and KPNO observations is given in Tomkin & Fekel (2006).

Finally, from 2003 through 2013, we collected an extensive number of spectra with the Tennessee State University 2 m Automatic Spectroscopic Telescope (AST) and a fiber-fed echelle spectrograph, situated at Fairborn Observatory near Washington Camp in the Patagonia Mountains of southeastern Arizona (Eaton & Williamson 2004, 2007). Through 2011 June the detector was a 2048×4096 SITe ST-002A CCD with $15\,\mu$m pixels. Eaton & Williamson (2007) have discussed reduction of the raw spectra and their wavelength calibration. Those AST echelle spectrograms have 21 orders that cover the wavelength range 4920–7100 Å with an average resolution of 0.17 Å. The typical signal-to-noise ratio of these observations is ∼80 at 6000 Å.

In the summer of 2011 the SITe CCD detector and dewar were replaced with a Fairchild 486 CCD with a 4000×4000 array of $15\,\mu$m pixels, which required a new readout electronics package, and a new dewar (Fekel et al. 2013). The echelle spectrograms that were obtained with this new detector have 48 orders, covering the wavelength range 3800–8260 Å. Because different diameter fibers were used at various times, the resolution of the new echelle spectra is either 0.24 or 0.4 Å, which resulted in signal-to-noise ratios that ranged from 80 to 150 at 6000 Å.

Tomkin & Fekel (2006) have discussed in detail the procedures that we have used to measure the McDonald and KPNO radial velocities. While the McDonald velocities are on an absolute scale, the KPNO velocities are relative velocities that have been determined by cross-correlation with respect to stars with constant radial velocities. For the KPNO red wavelength spectra, we used the IAU standards 10 Tau, HR 5694, and HR 7560 with velocities adopted from Scarfe et al. (1990). For the blue wavelength spectra, we employed several early-A stars, 68 Tau, HR 7773, and HR 8404, from a list of such stars that have been observed to identify constant velocity early-type stars (Fekel 1999). From our unpublished observations, our adopted velocities for those three stars are 39.0, −1.1, and 0.1 km s^{-1}, respectively.

Fekel et al. (2009b) provided an extensive general description of velocity measurement of the Fairborn AST spectra. The fact that HR 1528 is an Am star enabled us to use our line list for solar-type stars, which includes mostly neutral Fe lines, while for HR 6993 and 18 Vul we chose our line list for early- and mid-A type stars, which consists mostly of singly ionized lines of Fe, Si, and Ti. The lines of the 2 Sge short-period binary are narrow, enabling both components to be measured with either the solar or A-star line lists. Because we spectroscopically detected lines of the much fainter *Hipparcos* close visual companion, which could only be measured with the solar line list, we chose to measure all three components of 2 Sge with that list. A Gaussian function, which is quite adequate to fit the features of narrow-lined stars, was used to determine the velocities of HR 1528 and

HR 6993. However, because of the significantly larger rotational broadening of the 18 Vul components and the blending problems that sometimes occurred in the 2 Sge system because of lines of the third component, we used a rotational broadening function (Lacy & Fekel 2011) to fit the lines of those systems.

Like the velocities from McDonald, the resulting Fairborn velocities are absolute rather than relative velocities. Our unpublished measurements of several IAU standard solar-type stars indicate that the Fairborn Observatory velocities taken with the SITe CCD have a small zero-point offset of −0.3 km s^{-1} relative to the velocities of Scarfe et al. (1990). Starting in the fall of 2011, velocities from spectra obtained with the new CCD system have a zero-point offset −0.6 km s^{-1} relative to those of Scarfe et al. (1990). Thus, we added either 0.3 or 0.6 km s^{-1}, depending on which detector was used, to each measured velocity.

Fekel et al. (2011a) reaffirmed that despite the different methods of reduction, the KPNO velocities are on the same scale as the absolute velocities of McDonald to within a precision of 0.1–0.2 km s^{-1}, as was found by Tomkin & Fekel (2006). Thus, with the Fairborn zero-point corrections, the zero-point velocities of all three observatories should be essentially the same. Even if there was a more significant offset between the various data sets, it would simply slightly increase the uncertainty of the orbital elements since the number of Fairborn velocities of each system is at least three times larger than those from KPNO or McDonald.

4. DETERMINATION OF SPECTROSCOPIC ORBITS AND RESULTS

To determine the orbital elements we have used several computer programs. The program BISP (Wolfe et al. 1967), which implements a slightly modified version of the Wilsing–Russell method, has been used to determine initial orbits. With the differential corrections program SB1 (Barker et al. 1967), we then determined eccentric orbits. For a simultaneous solution of the two components, we used SB2, which is a slightly modified version of SB1. Finally, when appropriate, we computed circular orbits with the differential corrections programs SB1C and SB2C (D. Barlow 1998, private communication).

As mentioned earlier, our new spectra have been acquired at three observatories. The various detectors that we have used have different wavelength ranges, and so different numbers of lines have been measured to determine an average radial velocity. Also, the binary components usually have unequal line strengths and/or widths. These differences produce unequal velocity precisions. Therefore, when possible, we computed individual orbital solutions for the data sets of each component from each observatory. The variances of those individual solutions are inversely proportional to the weights that we assigned to the velocities in those different sets.

4.1. HR 1528

At Fairborn Observatory between 2003 and 2013, we acquired 95 spectrograms that show double lines. An additional 10 observations were obtained from 2004 to 2007 at McDonald Observatory and from 2006 through 2008 five more at KPNO were also collected. All of our new velocities are listed in Table 2.

To confirm the conclusion of Luyten (1936) and Stockton & Fekel (1992) that the orbit is circular, we analyzed the numerous Fairborn velocities of the much stronger primary lines. The resulting eccentricity of 0.00051 ± 0.00033 is very small and

Table 2
Radial Velocities of HR 1528

Hel. Julian Date (HJD − 2,400,000)	Phase	V_1 (km s^{-1})	$(O − C)_1$ (km s^{-1})	Wt$_1$	V_2 (km s^{-1})	$(O − C)_2$ (km s^{-1})	Wt$_2$	Source[a]
52966.931	0.931	70.6	−0.1	1.0	−64.9	0.5	0.07	Fair
52967.958	0.077	69.4	0.1	1.0	−63.6	−0.4	0.07	Fair
53031.806	0.132	56.7	0.0	1.0	−44.3	−0.2	0.07	Fair
53057.810	0.821	42.1	0.0	1.0	−22.2	−0.1	0.07	Fair
53108.605	0.025	75.4	0.0	0.8	−73.0	−0.4	0.02	McD
53109.635	0.171	45.1	0.0	0.8	−27.0	−0.5	0.02	McD
53277.810	0.022	75.5	0.0	1.0	−72.6	0.1	0.07	Fair
53287.031	0.330	−12.0	0.0	1.0	59.9	−0.3	0.07	Fair
53293.008	0.178	42.6	−0.1	1.0	−22.1	0.8	0.07	Fair
53301.994	0.452	−40.0	0.1	1.0	103.6	0.7	0.07	Fair
53311.915	0.859	54.2	−0.2	1.0	−41.1	−0.5	0.07	Fair
53313.007	0.014	75.9	0.0	1.0	−74.0	−0.7	0.07	Fair
53319.927	0.996	76.1	0.0	1.0	−73.9	−0.3	0.07	Fair
53334.059	1.000	75.9	−0.2	1.0	−74.3	−0.7	0.07	Fair
53340.886	0.968	75.0	0.1	1.0	−71.5	0.3	0.07	Fair
53351.930	0.535	−41.3	0.1	1.0	105.3	0.5	0.07	Fair
53358.786	0.507	−42.9	−0.2	1.0	106.5	−0.3	0.07	Fair
53385.889	0.351	−18.7	−0.2	1.0	69.3	−0.8	0.07	Fair
53395.880	0.768	23.5	0.2	1.0	6.2	−0.4	0.07	Fair
53400.738	0.457	−40.5	0.1	0.8	103.1	−0.5	0.02	McD
53401.757	0.601	−31.1	0.0	0.8	89.1	−0.1	0.02	McD
53489.598	0.060	72.0	0.0	0.8	−67.6	−0.2	0.02	McD
53662.946	0.645	−20.0	−0.2	0.8	70.4	−1.7	0.02	McD
53663.852	0.773	25.6	0.3	0.8	6.0	2.5	0.02	McD
53774.661	0.489	−42.6	0.0	0.8	106.3	−0.4	0.02	McD
53775.668	0.632	−23.5	0.0	0.8	77.4	−0.3	0.02	McD
54002.968	0.869	56.9	−0.2	0.8	−44.9	−0.2	0.02	KPNO
54003.928	0.005	76.1	0.0	0.8	−73.1	0.5	0.02	KPNO
54106.717	0.583	−34.8	0.0	0.8	94.4	−0.4	0.02	McD
54364.920	0.203	34.0	0.2	0.8	−8.9	0.5	0.02	KPNO
54369.956	0.918	67.9	−0.4	0.8	−61.3	0.5	0.02	KPNO
54526.659	0.142	53.9	0.0	0.8	−40.8	−0.9	0.02	KPNO
55241.774	0.564	−38.3	−0.3	1.0	99.4	−0.2	0.07	Fair
55276.730	0.522	−42.0	0.2	1.0	105.4	−0.7	0.07	Fair
55290.685	0.501	−42.8	0.0	1.0	107.0	0.1	0.07	Fair
55302.619	0.194	37.1	−0.1	1.0	−15.3	−0.8	0.07	Fair
55478.744	0.173	44.2	−0.1	1.0	−24.8	0.5	0.07	Fair
55485.981	0.200	35.1	−0.1	1.0	−12.2	−0.7	0.07	Fair
55498.011	0.906	65.9	−0.1	1.0	−59.2	−1.0	0.07	Fair
55513.935	0.164	47.2	0.0	1.0	−29.6	0.1	0.07	Fair
55521.925	0.297	−0.8	0.0	1.0	43.0	−0.1	0.07	Fair
55544.984	0.568	−37.8	−0.3	1.0	99.5	0.6	0.07	Fair
55565.889	0.533	−41.5	0.0	1.0	105.1	0.1	0.07	Fair
55573.910	0.670	−12.0	−0.1	1.0	59.3	−0.8	0.07	Fair
55579.801	0.506	−42.7	0.0	1.0	106.9	0.0	0.07	Fair
55586.821	0.501	−42.8	0.0	1.0	107.7	0.8	0.07	Fair
55600.833	0.489	−42.5	0.1	1.0	106.3	−0.4	0.07	Fair
55618.744	0.029	75.0	−0.1	1.0	−73.1	−0.9	0.07	Fair
55626.772	0.167	46.2	0.1	1.0	−28.8	−0.7	0.07	Fair
55635.647	0.426	−36.6	−0.1	1.0	96.7	−0.7	0.07	Fair
55645.676	0.848	51.2	0.1	1.0	−35.3	0.4	0.07	Fair
55651.691	0.702	−1.2	0.0	1.0	42.8	−0.9	0.07	Fair
55842.826	0.810	38.4	0.0	1.0	−17.0	−0.6	0.07	Fair
55848.868	0.666	−13.2	−0.1	1.0	61.6	−0.3	0.07	Fair
55854.768	0.503	−42.9	−0.1	1.0	106.9	0.0	0.07	Fair
55862.830	0.647	−19.4	−0.1	1.0	70.8	−0.4	0.07	Fair
55882.781	0.476	−41.9	0.2	1.0	106.4	0.5	0.07	Fair
55893.867	0.049	73.2	−0.2	1.0	−69.4	0.1	0.07	Fair
55903.876	0.468	−41.4	0.2	1.0	105.5	0.4	0.07	Fair
55921.670	0.992	76.0	0.0	1.0	−73.1	0.4	0.07	Fair
55929.872	0.155	49.9	−0.2	1.0	−34.0	0.1	0.07	Fair
55932.933	0.589	−33.7	0.0	1.0	92.6	−0.5	0.07	Fair
55936.918	0.154	50.3	0.0	1.0	−34.1	0.3	0.07	Fair
55946.801	0.556	−39.2	−0.1	1.0	102.0	0.6	0.07	Fair

Table 2
(Continued)

Hel. Julian Date (HJD − 2,400,000)	Phase	V_1 (km s^{-1})	$(O-C)_1$ (km s^{-1})	Wt$_1$	V_2 (km s^{-1})	$(O-C)_2$ (km s^{-1})	Wt$_2$	Source[a]
55955.802	0.833	46.2	0.1	1.0	−28.1	0.0	0.07	Fair
55962.858	0.833	46.2	−0.2	1.0	−28.6	−0.1	0.07	Fair
55970.830	0.964	74.6	0.0	1.0	−71.2	0.1	0.07	Fair
55977.701	0.938	71.8	0.1	1.0	−66.2	0.8	0.07	Fair
55984.690	0.930	70.5	0.1	1.0	−64.6	0.4	0.07	Fair
55996.756	0.641	−21.3	−0.3	1.0	74.3	0.5	0.07	Fair
56016.675	0.466	−41.5	−0.1	1.0	105.2	0.3	0.07	Fair
56027.648	0.022	75.5	0.0	1.0	−73.0	−0.3	0.07	Fair
56029.657	0.307	−4.5	−0.3	1.0	48.9	0.5	0.07	Fair
56193.789	0.585	−34.5	−0.1	1.0	94.3	0.1	0.07	Fair
56200.849	0.587	−34.2	0.0	1.0	93.7	−0.2	0.07	Fair
56203.917	0.022	75.5	0.0	1.0	−72.6	0.2	0.07	Fair
56210.890	0.011	75.8	−0.2	1.0	−73.6	−0.2	0.07	Fair
56215.737	0.698	−2.1	0.2	1.0	45.8	0.3	0.07	Fair
56217.876	0.002	76.1	0.0	1.0	−74.0	−0.4	0.07	Fair
56223.872	0.852	52.1	−0.1	1.0	−37.5	−0.2	0.07	Fair
56225.697	0.111	62.2	−0.1	1.0	−53.6	−1.0	0.07	Fair
56226.858	0.275	7.3	0.1	1.0	32.0	0.9	0.07	Fair
56229.838	0.698	−2.3	0.1	1.0	46.0	0.4	0.07	Fair
56231.681	0.960	74.3	0.1	1.0	−70.3	0.4	0.07	Fair
56232.694	0.103	64.0	0.0	1.0	−55.8	−0.5	0.07	Fair
56236.835	0.690	−5.0	0.1	1.0	49.7	0.1	0.07	Fair
56237.825	0.831	45.7	0.1	1.0	−27.0	0.3	0.07	Fair
56243.036	0.570	−37.0	0.1	1.0	98.9	0.5	0.07	Fair
56250.642	0.649	−18.7	0.0	1.0	70.3	0.0	0.07	Fair
56255.888	0.393	−29.7	0.1	1.0	86.8	−0.4	0.07	Fair
56260.761	0.084	68.0	0.0	1.0	−61.6	−0.2	0.07	Fair
56264.916	0.673	−11.0	0.0	1.0	58.6	0.0	0.07	Fair
56266.864	0.949	73.1	0.0	1.0	−68.0	1.1	0.07	Fair
56267.848	0.089	67.1	0.1	1.0	−60.5	−0.6	0.07	Fair
56272.838	0.797	33.9	0.1	1.0	−9.5	−0.1	0.07	Fair
56273.830	0.937	71.8	0.2	1.0	−66.1	0.6	0.07	Fair
56274.850	0.082	68.5	0.1	1.0	−62.3	−0.4	0.07	Fair
56281.737	0.059	72.2	0.1	1.0	−66.9	0.6	0.07	Fair
56288.882	0.072	70.3	0.2	1.0	−64.1	0.4	0.07	Fair
56295.930	0.072	70.4	0.2	1.0	−64.1	0.5	0.07	Fair
56302.929	0.064	71.6	0.3	1.0	−65.7	0.6	0.07	Fair
56310.889	0.193	37.4	0.0	1.0	−15.0	−0.2	0.07	Fair
56311.874	0.333	−12.9	0.1	1.0	61.2	−0.4	0.07	Fair
56324.849	0.173	44.0	−0.2	1.0	−24.9	0.3	0.07	Fair
56331.825	0.163	47.7	0.0	1.0	−29.7	0.8	0.07	Fair
56340.815	0.438	−38.0	0.3	1.0	100.6	0.5	0.07	Fair
56348.802	0.570	−37.1	0.0	1.0	97.8	−0.4	0.07	Fair
56349.798	0.712	2.5	0.0	1.0	38.8	0.6	0.07	Fair
56358.760	0.983	75.6	−0.1	1.0	−73.3	−0.2	0.07	Fair
56384.686	0.660	−15.4	−0.1	1.0	65.1	−0.1	0.07	Fair

Note. [a] Fair = Fairborn Observatory, McD = McDonald Observatory, KPNO = Kitt Peak National Observatory.

consistent with the assumption of a circular orbit (Lucy & Sweeney 1971). Because of the small number of velocities from McDonald and especially KPNO, we combined the velocities from those two observatories and obtained separate circular orbit solutions for the primary and secondary. Two more independent circular orbit solutions were computed with the Fairborn velocities, one for each component. From those results we determined weights of 1.0, 0.8, and 0.8 for the Fairborn, McDonald, and KPNO velocities of the primary, respectively, and 0.07, 0.02, and 0.02 for the secondary velocities from the same three observatories. The four individual solutions have center-of-mass velocities within 0.2 km s^{-1} of each other. Thus, we computed a simultaneous circular orbit solution of

the weighted primary and secondary velocities from the three observatories, which produced a period of 7.050869 days.

In principle, earlier radial velocities of HR 1528 could be used to improve the precision of the period and possibly the other elements. Thus, we examined the KPNO primary velocities of Stockton & Fekel (1992). An orbital solution of those data alone produces a center-of-mass velocity that differs by 1.2 km s^{-1} from the solution of our new data, and results in weights of 0.03 for the observations. Combining those velocities, shifted by −1.2 km s^{-1}, with our new velocities from Fairborn, McDonald, and KPNO, we obtained a circular solution with orbital elements that do not differ significantly from the elements computed with just our new velocities. In particular, the period, whose precision

Table 3
Orbital Elements and Related Parameters of HR 1528

| Parameter	Stockton & Fekel (1992)	This Study
P (days)	7.050933 ± 0.000024	7.0508687 ± 0.0000023
T_0 (HJD)	2448158.713	$2454673.72440 \pm 0.00043$
e	0.0 (adopted)	0.0 (adopted)
K_1 (km s^{-1})	58.9 ± 0.3	59.442 ± 0.017
K_2 (km s^{-1})	89.7 ± 0.7	90.283 ± 0.065
γ (km s^{-1})	17.8 ± 0.1	16.654 ± 0.012
$m_1 \sin^3 i$ ($M_\odot$)	1.45 ± 0.02	1.4786 ± 0.0024
$m_2 \sin^3 i$ ($M_\odot$)	0.95 ± 0.01	0.9735 ± 0.0010
$a_1 \sin i$ (10^6 km)	5.71 ± 0.03	5.7633 ± 0.0016
$a_2 \sin i$ (10^6 km)	8.70 ± 0.07	8.7536 ± 0.0063
Standard error of an unit weight observation (km s^{-1})	$\cdots$	0.13
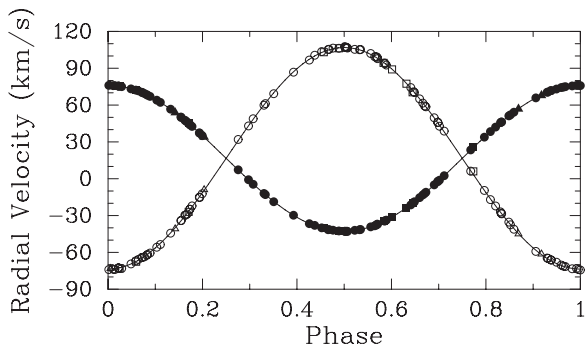
Figure 1. Radial velocities of HR 1528 compared with the computed velocity curves. Filled and open symbols represent the primary and secondary, respectively. Circles = Fairborn Observatory, triangles = KPNO, and squares = McDonald Observatory. Zero phase is a time of maximum velocity of the primary.

Figure 2. HR 1528 radial velocity residuals vs. orbital phase. Panel (a) shows residuals of the primary, while panel (b) is of the secondary. Circles = Fairborn Observatory, triangles = KPNO, and squares = McDonald Observatory. Zero phase is a time of maximum velocity of the primary.

could benefit from the longer time span of the four data sets, is changed by less than 1σ. Thus, we have chosen to adopt the simultaneous circular orbit solution, determined with only our new primary and secondary velocities. Table 3 lists those elements. For a circular orbit the element T, a time of periastron passage, is undefined. Thus, as recommended by Batten et al. (1989), T_0, a time of maximum velocity for the primary, is used instead. Figure 1 compares our primary and secondary velocities from our three observatories with the calculated velocity curves. Figure 2 plots the velocity residuals versus phase for the primary and secondary. As expected from the large magnitude difference between the two components (Section 5.1), the typical residual of the secondary is much greater than that of the primary.

In addition to our new elements, Table 3 lists the elements of Stockton & Fekel (1992). A comparison shows that the values of the elements are in good agreement, but our newly derived elements are five to 10 times more precise. The systemic velocities of the two solutions in Table 3 differ by 1.2 km s^{-1}, -17.8 ± 0.1 km s^{-1} versus -16.65 ± 0.01 km s^{-1}.

One additional set of velocities is available for examination. A recomputation of the orbit with the use of the DAO photographic plate velocities (Harper 1932a) results in a center-of-mass velocity of -20.5 ± 0.9 km s^{-1}. Eliminating two DAO velocities that have very large residuals revises that systemic velocity to -20.6 ± 0.6 km s^{-1}. Thus, the orbital solutions indicate that the center-of-mass velocity of HR 1528 has a range of 4 km s^{-1}. Observatory zero-point velocity differences are usually in the 1–2 km s^{-1} range (e.g., Harper 1932b). Therefore, the difference between the DAO and the more recent data sets suggests that there is a third component in the system. Taken at face value, the velocity change validates the interferometric discovery of
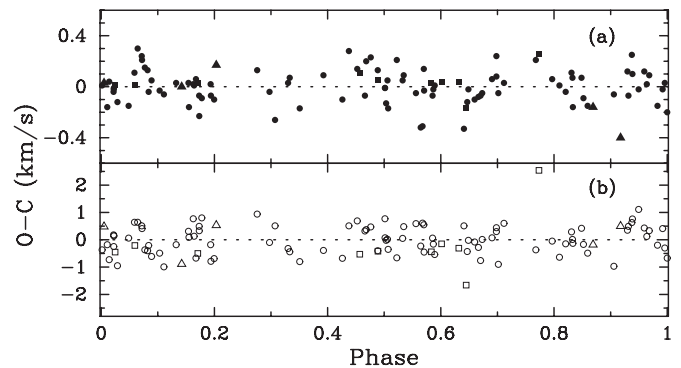
a third component (McAlister et al. 1987). However, despite this apparent spectroscopic confirmation, questions remain because over more than a quarter century, there has been no interferometric confirmation of the wider binary. As an additional test of our spectroscopic data, we divided the time span of our Fairborn data in half and computed orbits for the primary velocities of both sets. The two systemic velocities are identical, showing no evidence of orbital motion during the 9.4 yr covered by our new observations.

4.2. HR 6993

Between 2002 and 2013 we obtained a total of 119 spectroscopic observations of HR 6993 at three observatories. We began our observing program at McDonald Observatory, acquiring a dozen spectrograms between 2002 and 2005. From 2004 through 2011, we collected 26 observations at KPNO. Finally, from 2004 through 2013, we also observed HR 6993 at Fairborn Observatory, where we obtained 81 usable double-lined spectrograms (Table 4). The number of velocities at each of the three observatories is large enough that we initially analyzed each data set separately, obtaining six orbital solutions, three for the primary and three for the secondary. The variances of the three orbital solutions for the primary resulted in weights of 1.0, 0.4, and 0.2 for the velocities from McDonald, Fairborn, and KPNO, respectively. For the secondary, the weights were 0.2, 0.2, and 0.1 for the same three respective observatories. The center-of-mass velocities of the six data sets agree to within 0.4 km s^{-1}. So, we next obtained a simultaneous solution of all our velocities, which produced an orbital period of 14.68463 days.

Table 4
Radial Velocities of HR 6993

Hel. Julian Date (HJD − 2,400,000)	Phase	V_1 (km s^{-1})	$(O - C)_1$ (km s^{-1})	Wt$_1$	V_2 (km s^{-1})	$(O - C)_2$ (km s^{-1})	Wt$_2$	Source[a]
52392.912	0.975	−25.6	−0.2	1.0	48.5	−0.4	0.2	McD
52749.948	0.289	42.9	−0.5	1.0	−21.1	0.0	0.2	McD
52750.939	0.356	41.0	−0.6	1.0	−19.3	0.0	0.2	McD
52888.727	0.739	−7.7	−0.1	1.0	30.5	−0.3	0.2	McD
52889.698	0.805	−20.2	−0.2	1.0	43.5	0.2	0.2	McD
53075.004	0.424	36.6	−0.3	1.0	−14.8	−0.3	0.2	McD
53110.913	0.870	−30.0	−0.2	1.0	53.3	−0.1	0.2	McD
53168.840	0.815	−22.0	−0.4	0.2	45.2	0.2	0.1	KPNO
53169.873	0.885	−31.3	0.0	0.2	54.4	−0.4	0.1	KPNO
53171.842	0.019	−11.7	0.3	0.2	35.9	0.7	0.1	KPNO
53259.633	0.997	−19.4	−0.1	1.0	42.6	0.0	0.2	McD
53261.740	0.141	28.8	−0.1	1.0	−6.2	0.1	0.2	McD
53276.640	0.156	32.1	0.1	0.4	−8.4	1.1	0.2	Fair
53285.683	0.771	−13.2	0.4	0.4	36.9	0.0	0.2	Fair
53290.669	0.111	21.4	0.4	0.4	2.3	0.6	0.2	Fair
53302.665	0.928	−31.8	0.3	0.4	55.2	−0.5	0.2	Fair
53314.629	0.743	−7.9	0.3	0.4	30.7	−0.7	0.2	Fair
53423.020	0.124	25.5	0.9	0.4	−0.8	1.2	0.2	Fair
53470.939	0.387	39.9	0.1	0.4	−17.6	−0.2	0.2	Fair
53483.831	0.265	43.1	0.0	0.4	−21.3	−0.5	0.2	Fair
53486.937	0.476	31.6	−0.4	1.0	−9.5	0.0	0.2	McD
53489.896	0.678	3.5	0.0	1.0	19.4	0.0	0.2	McD
53490.952	0.750	−9.8	−0.2	0.2	33.0	0.2	0.1	KPNO
53496.970	0.160	33.3	0.5	0.4	−9.4	0.9	0.2	Fair
53509.940	0.043	−2.6	0.4	0.4	26.0	−0.1	0.2	Fair
53528.887	0.333	42.6	0.0	0.4	−19.9	0.4	0.2	Fair
53536.923[b]	0.880	−31.1	−0.2	0.2	53.6	−0.9	0.1	KPNO
53548.906	0.696	1.1	0.8	0.4	23.5	0.8	0.2	Fair
53563.798	0.711	−2.3	0.0	0.4	25.2	−0.1	0.2	Fair
53608.684	0.767	−12.7	0.2	0.4	35.0	−1.1	0.2	Fair
53629.741	0.201	39.1	0.1	0.4	−15.9	0.7	0.2	Fair
53638.599[b]	0.804	−20.3	−0.5	0.2	42.8	−0.3	0.1	KPNO
53663.557	0.504	28.6	−0.3	1.0	−7.0	−0.6	0.2	McD
53673.638	0.190	37.6	−0.1	0.4	−14.6	0.7	0.2	Fair
53846.883	0.988	−21.9	0.1	0.4	45.8	0.4	0.2	Fair
53851.951	0.333	41.8	−0.8	0.2	−20.7	−0.4	0.1	KPNO
53859.985	0.880	−30.7	0.2	0.4	54.8	0.3	0.2	Fair
53872.824	0.755	−10.0	0.5	0.4	33.4	−0.3	0.2	Fair
53902.910	0.804	−19.5	0.1	0.4	43.2	0.2	0.2	Fair
53996.768	0.195	38.6	0.3	0.4	−16.4	−0.5	0.2	Fair
54005.611[b]	0.797	−18.9	−0.4	0.2	41.9	0.1	0.1	KPNO
54022.646	0.957	−28.9	0.1	0.4	52.6	0.1	0.2	Fair
54268.918[b]	0.728	−4.8	0.7	0.2	28.7	0.1	0.1	KPNO
54269.856	0.792	−18.5	−1.0	0.2	39.9	−0.9	0.1	KPNO
54364.610	0.245	41.7	−0.6	0.2	−18.9	1.2	0.1	KPNO
54582.961	0.114	21.2	−0.6	0.2	0.6	−0.2	0.1	KPNO
54586.926[b]	0.384	39.6	−0.4	0.2	−18.1	−0.5	0.1	KPNO
54643.882	0.263	42.4	−0.6	0.2	−21.0	−0.3	0.1	KPNO
54947.966	0.970	−27.1	−0.6	0.2	48.8	−1.2	0.1	KPNO
54950.941	0.173	34.1	−1.0	0.2	−12.7	0.0	0.1	KPNO
55006.916	0.985	−22.0	1.0	0.2	47.6	1.2	0.1	KPNO
55094.670	0.960	−27.3	1.1	0.2	52.7	0.8	0.1	KPNO
55246.010	0.266	43.3	0.2	0.4	−20.5	0.3	0.2	Fair
55274.896	0.234	41.8	0.1	0.4	−19.5	−0.1	0.2	Fair
55284.004	0.854	−27.5	0.3	0.4	51.2	−0.1	0.2	Fair
55293.881	0.526	26.0	−0.2	0.4	−2.6	1.0	0.2	Fair
55312.935	0.824	−23.2	0.0	0.4	47.1	0.5	0.2	Fair
55312.953	0.825	−23.9	−0.5	0.2	46.0	−0.8	0.1	KPNO
55314.985	0.964	−28.6	−0.7	0.2	49.9	−1.5	0.1	KPNO
55320.808	0.360	42.2	0.8	0.4	−18.7	0.4	0.2	Fair
55329.965	0.984	−23.1	0.1	0.4	47.2	0.5	0.2	Fair
55341.931	0.799	−18.5	0.2	0.4	42.3	0.2	0.2	Fair
55370.920	0.773	−13.4	0.5	0.2	37.0	−0.1	0.1	KPNO
55376.940	0.183	36.5	−0.1	0.4	−13.8	0.4	0.2	Fair

Table 4
(Continued)

Hel. Julian Date (HJD − 2,400,000)	Phase	V_1 (km s^{-1})	$(O - C)_1$ (km s^{-1})	Wt$_1$	V_2 (km s^{-1})	$(O - C)_2$ (km s^{-1})	Wt$_2$	Source[a]
55385.873	0.791	−17.3	0.0	0.4	39.7	−0.9	0.2	Fair
55451.681	0.272	43.9	0.7	0.4	−20.4	0.5	0.2	Fair
55458.682	0.749	−9.0	0.4	0.4	32.8	0.2	0.2	Fair
55469.648	0.496	29.8	0.0	0.4	−6.6	0.7	0.2	Fair
55477.652	0.041	−2.9	0.9	0.4	27.1	0.2	0.2	Fair
55488.645	0.790	−16.8	0.2	0.4	40.6	0.2	0.2	Fair
55623.948	0.003	−17.3	0.1	0.4	41.5	0.8	0.2	Fair
55635.004	0.756	−10.3	0.5	0.4	34.2	0.2	0.2	Fair
55643.894	0.362	42.0	0.7	0.4	−19.1	−0.1	0.2	Fair
55649.896	0.770	−13.4	0.1	0.4	37.2	0.5	0.2	Fair
55656.951	0.251	43.1	0.5	0.4	−20.0	0.3	0.2	Fair
55664.841	0.788	−17.2	−0.4	0.4	40.1	0.0	0.2	Fair
55670.861	0.198	38.6	0.0	0.4	−15.7	0.6	0.2	Fair
55674.927	0.475	32.3	0.2	0.4	−10.1	−0.5	0.2	Fair
55678.821	0.740	−8.0	−0.2	0.4	30.8	−0.1	0.2	Fair
55679.926	0.815	−22.3	−0.6	0.2	43.7	−1.4	0.1	KPNO
55680.944	0.885	−32.2	−0.9	0.2	54.1	−0.7	0.1	KPNO
55681.934	0.952	−30.6	−0.8	0.2	52.6	−0.7	0.1	KPNO
55684.861	0.152	31.8	0.6	0.4	−8.3	0.4	0.2	Fair
55688.803	0.420	37.7	0.4	0.4	−15.0	−0.1	0.2	Fair
55694.800	0.828	−24.2	−0.3	0.4	47.9	0.5	0.2	Fair
55699.784	0.168	34.5	0.2	0.4	−11.9	−0.1	0.2	Fair
55716.737	0.322	42.9	0.0	0.4	−20.9	−0.3	0.2	Fair
55724.954	0.882	−31.1	−0.1	0.4	54.2	−0.4	0.2	Fair
55730.810	0.281	42.8	−0.5	0.2	−21.4	−0.3	0.1	KPNO
55732.850	0.419	36.6	−0.7	0.2	−15.5	−0.5	0.1	KPNO
55743.861	0.169	34.2	−0.3	0.4	−12.7	−0.6	0.2	Fair
55846.666	0.170	34.2	−0.5	0.4	−11.6	0.6	0.2	Fair
55954.036	0.482	32.0	0.6	0.4	−8.7	0.2	0.2	Fair
55976.012	0.978	−24.8	−0.2	0.4	48.7	0.7	0.2	Fair
55993.002	0.135	27.2	−0.4	0.4	−5.3	−0.3	0.2	Fair
56011.977	0.428	37.2	0.5	0.4	−14.6	−0.3	0.2	Fair
56017.951	0.834	−24.8	0.1	0.4	48.7	0.3	0.2	Fair
56046.784	0.798	−19.2	−0.6	0.4	42.8	0.9	0.2	Fair
56055.979	0.424	37.1	0.1	0.4	−15.3	−0.7	0.2	Fair
56061.833	0.823	−23.3	−0.3	0.4	47.0	0.6	0.2	Fair
56062.796	0.888	−31.6	−0.1	0.4	55.0	−0.1	0.2	Fair
56063.798	0.957	−29.2	−0.1	0.4	52.2	−0.4	0.2	Fair
56067.774	0.227	41.7	0.4	0.4	−20.1	−1.1	0.2	Fair
56074.766	0.703	−0.5	0.5	0.4	24.7	0.7	0.2	Fair
56077.773	0.908	−32.2	0.2	0.4	55.2	−0.8	0.2	Fair
56082.756	0.248	42.6	0.1	0.4	−20.6	−0.4	0.2	Fair
56095.912	0.143	29.8	0.4	0.4	−7.4	−0.5	0.2	Fair
56100.736	0.472	32.8	0.4	0.4	−10.0	0.0	0.2	Fair
56126.912	0.254	41.9	−0.9	0.4	−20.8	−0.3	0.2	Fair
56213.655	0.162	32.6	−0.5	0.4	−10.4	0.3	0.2	Fair
56228.642	0.182	36.1	−0.4	0.4	−14.8	−0.7	0.2	Fair
56347.017	0.243	42.1	−0.2	0.4	−20.8	−0.8	0.2	Fair
56389.900	0.164	33.7	0.2	0.4	−11.6	−0.5	0.2	Fair
56400.853	0.909	−32.0	0.4	0.4	55.9	−0.1	0.2	Fair
56405.845	0.249	42.9	0.3	0.4	−21.6	−1.3	0.2	Fair
56406.863	0.319	43.6	0.6	0.4	−21.8	−1.1	0.2	Fair
56409.819	0.520	27.3	0.3	0.4	−4.1	0.3	0.2	Fair
56414.835	0.862	−28.8	0.0	0.4	51.7	−0.7	0.2	Fair
56419.797	0.199	39.2	0.4	0.4	−17.0	−0.6	0.2	Fair

Notes.

[a] McD = McDonald Observatory, KPNO = Kitt Peak National Observatory, Fair = Fairborn Observatory.

[b] Blue wavelength spectrum.

The only other extensive velocity data set is that of Petrie (1948), who, over the course of just under 12 months, obtained at the DAO 17 double-lined spectrograms with a linear dispersion of 11 Å mm^{-1} at Hγ. Despite this relatively high dispersion and the narrow lines of the two components, an average of just six lines per component was measured on each plate. The precision of the better primary velocities is very poor, with a solution of those velocities producing relative weights of less
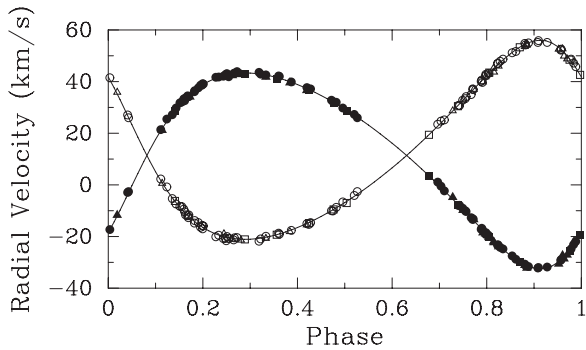
Figure 3. Radial velocities of HR 6993 compared with the computed velocity curves. Filled and open symbols represent the primary and secondary, respectively. Circles = Fairborn Observatory, triangles = KPNO, and squares = McDonald Observatory. Zero phase is a time of periastron passage.
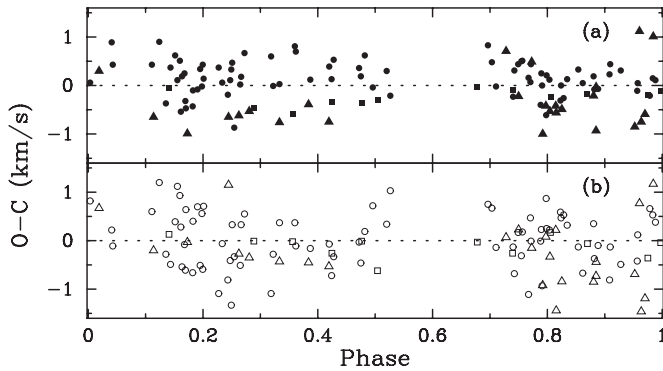

Figure 4. HR 6993 radial velocity residuals vs. orbital phase. Panel (a) shows residuals of the primary, while panel (b) is of the secondary. Circles = Fairborn Observatory, triangles = KPNO, and squares = McDonald Observatory. Zero phase is a time of periastron passage.

than 0.01. Thus, we have not included the DAO velocities in our solution.

The new orbital elements from our double-lined solution are given in Table 5. Our primary and secondary velocities are compared with the computed velocity curves in Figure 3. In that plot, zero phase is a time of periastron passage. Figure 4 shows the velocity residuals versus phase for the primary and secondary. Although the magnitude difference between the two components is modest (Section 5.2), the typical residual of the secondary is somewhat greater than that of the primary.

For comparison, we also list in Table 5 the orbital elements of Petrie (1948). They are in general agreement with our much more precise results. However, our eccentricity is 18% larger, and we find that the stronger lined star, which Petrie called the primary, is as expected the slightly more massive one, which is the reverse of Petrie's result.

4.3. 2 Sge

Our observation of 2 Sge was begun at McDonald Observatory where we acquired 12 spectrograms between 2002 and 2005. From 2004 through 2012, we obtained 28 additional observations at KPNO. Our most extensive observing campaign was conducted at Fairborn Observatory. There between 2004 and 2013 we collected 85 usable spectrograms. A KPNO spectrum of 2 Sge in the 4500 Å region is shown in Figure 5. Clearly visible is the significant line strength difference between the short-period primary and secondary components. A KPNO red wavelength spectrum is presented in Figure 6 showing the weakness of the A-star lines in the 6430 Å region. Also seen are very
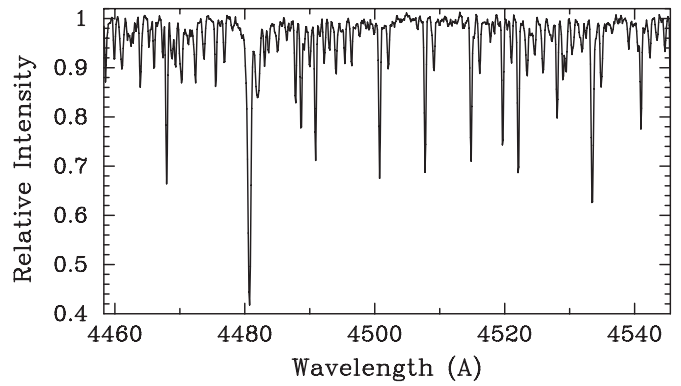

Figure 5. KPNO spectrum of the 4500 Å region of 2 Sge. It shows the narrow-lined nature of both short-period components as well as the large line strength difference between the strong short-period primary features and the much weaker secondary features. The strongest line in this region is the Mg II line at 4481 Å. Most of the other features are Fe II or Ti II lines.
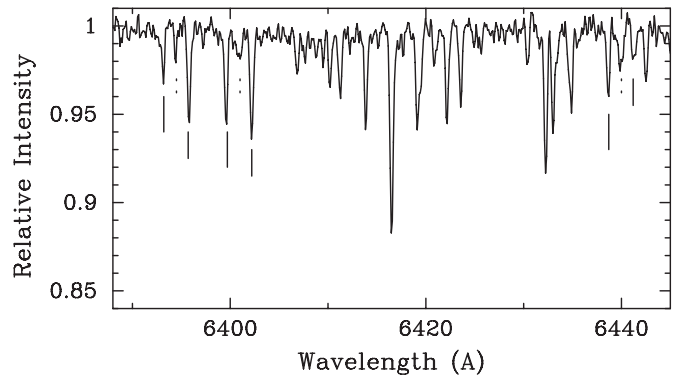

Figure 6. KPNO spectrum of the 6420 Å region of 2 Sge. Three sets of triple lines are indicated. Solid lines identify the short-period primary (longer line) and secondary (shorter line) components, while very weak features of the close visual component are identified by dashed lines. In this region for Fe I lines it is the secondary that is the stronger component. The triplet near 6440 Å is that of a Ca I line.

weak lines of the close visual companion that was discovered by the *Hipparcos* team (Perryman et al. 1997). Our new velocities of the short-period binary as well as those of the faint, close visual companion are given in Table 6.

The number of velocities of 2 Sge at each of the three observatories is large enough, and the orbital phase coverage is good enough so that just as we did with HR 6993, we initially analyzed each data set separately, obtaining six separate orbital solutions, three for the primary and three for the secondary. The eccentricity of each solution was very small, ranging from 0.004 to 0.011. However, the longitude of periastron values of the primary were similar and the values for the secondary differed by roughly 180° from those of the primary, indicating that the short-period orbit of 2 Sge does indeed have a very small eccentricity. Velocity residuals from the Fairborn orbit of the short-period secondary suggest that there might be a small $+0.3$ km s^{-1} shift in its center-of-mass velocity over the course of our observations, but that result was not confirmed in the other data sets. The center-of-mass velocities of the six solutions have a range of 0.6 km s^{-1}, and so we have chosen to combine all our velocities into a single simultaneous solution. From the six individual solutions the weights for the short-period primary are 1.0, 0.3, and 0.3 for the velocities from McDonald, KPNO, and Fairborn, respectively. For the secondary the weights are 1.0, 0.9, and 0.4 for the same three observatories. The

Table 5
Orbital Elements and Related Parameters of HR 6993

| Parameter	Petrie (1948)	This Study
P (days)	14.674 ± 0.007	14.684636 ± 0.000029
T (HJD)	2432304.628	2454405.073 ± 0.011
e	0.211 ± 0.012	0.2495 ± 0.0011
ω (deg)	224.9 ± 3.8	230.90 ± 0.30
K_1 (km s^{-1})	38.56 ± 0.53	37.918 ± 0.050
K_2 (km s^{-1})	38.07 ± 0.56	38.569 ± 0.076
γ (km s^{-1})	11.39 ± 0.35	11.415 ± 0.031
$m_1 \sin^3 i$ ($M_\odot$)	0.320	0.3118 ± 0.0012
$m_2 \sin^3 i$ ($M_\odot$)	0.324	0.3065 ± 0.0010
$a_1 \sin i$ (10^6 km)	7.621	7.414 ± 0.010
$a_2 \sin i$ (10^6 km)	7.522	7.542 ± 0.015
Standard error of an unit weight observation (km s^{-1})	. . .	0.25
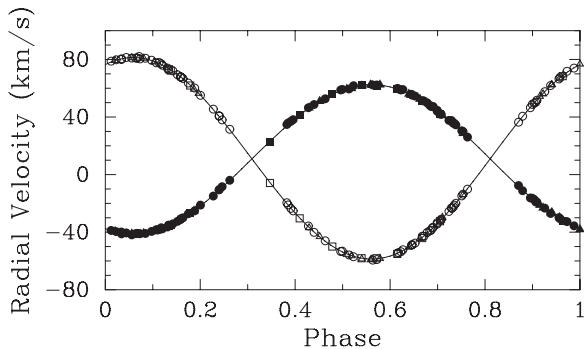
Figure 7. Radial velocities of 2 Sge compared with the computed velocity curves. Filled and open symbols represent the primary and secondary, respectively. Circles = Fairborn Observatory, triangles = KPNO, and squares = McDonald Observatory. Zero phase is a time of periastron passage.

Figure 8. 2 Sge radial velocity residuals vs. orbital phase. Panel (a) shows residuals of the primary, while panel (b) is of the secondary. Circles = Fairborn Observatory, triangles = KPNO, and squares = McDonald Observatory. Zero phase is a time of periastron passage.

Figure 9. Radial velocities of the close visual secondary of 2 Sge. Panel (a) plots the Fairborn Observatory radial velocities vs. Julian Date. Those velocities indicate a slight negative trend over time. Panel (b) presents the McDonald Observatory (solid squares) and KPNO (solid triangles) velocities, which do not confirm the trend suggested by the Fairborn velocities.

higher weights assigned to the KPNO and Fairborn secondary velocities reflect the fact that at red wavelengths the neutral Fe lines of the secondary are stronger than those of the primary.

The only other major velocity data set consists of the old photographic plate results from the Dominion Observatory in Ottawa (Young 1917). An orbital solution of those primary velocities produces a standard deviation per plate of 6.2 km s^{-1} resulting in such low weights for those velocities that they do not significantly improve the value of the period. Thus, the new orbital elements from our double-lined solution are given in Table 7. Our primary and secondary velocities are compared with the computed velocity curves in Figure 7. In that plot zero phase is a time of periastron passage. As seen in Figure 8, the stronger secondary lines in the KPNO and Fairborn spectra result in smaller velocity residuals for the secondary.

The orbital elements for 2 Sge, computed by Luyten (1936) from the Dominion Observatory velocities, are shown for comparison in Table 7. Given that the original solution of the Dominion Observatory velocities was described as preliminary (Young 1917), the circular orbital elements from those velocities are in reasonable agreement with our much more precise results.

Velocities of the faint, close visual secondary, discovered by the *Hipparcos* team (Perryman et al. 1997), are measurable if the spectrograms have a high enough signal-to-noise ratio. Those velocities (Table 6) are shown in a two-panel plot. In Figure 9, panel (a) presents the Fairborn velocities plotted versus Julian Date. When divided into three subsets, the one centered near
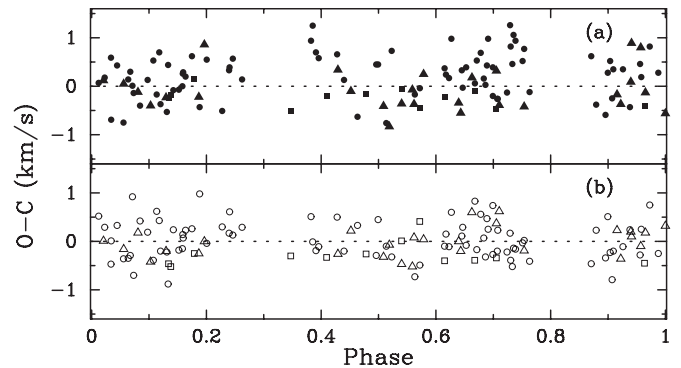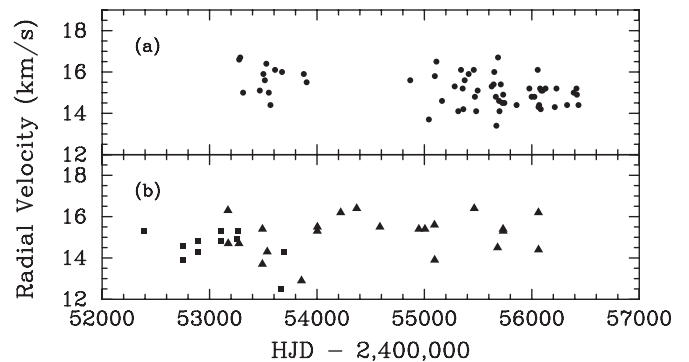
JD 2,453,500 has an average velocity of 15.7 km s^{-1} while the subset centered near JD 2,456,200 has an average of 14.9 km s^{-1}. Thus, these data indicate a velocity decrease of 0.8 km s^{-1} over the nearly 9 yr span of observation. Seeming to suggest possible orbital motion, this change is in the opposite direction to the 0.3 km s^{-1} shift found in the Fairborn velocity residuals of the short-period secondary, which was mentioned previously. Panel (b) plots our other two data sets, the McDonald and KPNO velocities. These velocities show no evidence of the change suggested by the Fairborn velocities. Thus, we conclude that any velocity change of the short-period binary center of mass and that of its close visual secondary remains to be confirmed.

Table 6
Radial Velocities of 2 Sge

Hel. Julian Date (HJD − 2,400,000)	Phase	V_1 (km s^{-1})	$(O-C)_1$ (km s^{-1})	Wt$_1$	V_2 (km s^{-1})	$(O-C)_2$ (km s^{-1})	Wt$_2$	V_3 (km s^{-1})	Source[a]
52391.934	0.134	−35.7	−0.3	1.0	73.2	−0.5	1.0	15.3	McD
52749.968	0.572	61.9	−0.4	1.0	−58.1	0.4	1.0	13.9	McD
52750.954	0.705	42.3	−0.5	1.0	−32.4	−0.3	1.0	14.6	McD
52888.745	0.347	22.6	−0.5	1.0	−5.8	−0.3	1.0	. . .	McD
52889.716	0.478	55.7	−0.2	1.0	−50.0	−0.3	1.0	14.8	McD
52890.727	0.615	59.3	−0.2	1.0	−55.1	−0.4	1.0	14.3	McD
53108.947	0.138	−35.0	−0.2	1.0	72.3	−0.5	1.0	14.8	McD
53110.955	0.410	41.1	−0.2	1.0	−30.4	−0.3	1.0	15.3	McD
53169.908	0.385	35.9	1.2	0.3	−21.1	0.0	0.4	. . .	Fair
53170.895	0.519	59.9	−0.8	0.3	−56.4	−0.1	0.9	16.3	KPNO
53173.877	0.922	−23.1	−0.4	0.3	56.1	−0.4	0.9	14.7	KPNO
53259.751	0.540	62.0	0.0	1.0	−58.1	0.0	1.0	14.9	McD
53260.694	0.668	51.3	−0.1	1.0	−44.1	−0.4	1.0	15.3	McD
53273.715	0.429	46.5	0.3	0.3	−36.9	−0.3	0.9	14.7	KPNO
53275.774	0.708	41.9	−0.3	0.3	−31.0	0.2	0.4	16.6	Fair
53285.737	0.056	−41.9	−0.7	0.3	81.0	−0.4	0.4	16.7	Fair
53290.723	0.730	36.9	0.8	0.3	−23.4	−0.4	0.4	. . .	Fair
53311.664	0.563	62.3	−0.2	0.3	−59.4	−0.7	0.4	. . .	Fair
53312.669	0.699	44.1	−0.2	0.3	−34.4	−0.3	0.4	15.0	Fair
53467.892	0.699	44.7	0.4	0.3	−33.4	0.7	0.4	15.1	Fair
53491.972	0.957	−29.8	0.8	0.3	67.0	−0.1	0.9	13.7	KPNO
53492.887	0.081	−40.8	−0.1	0.3	80.9	0.2	0.9	15.4	KPNO
53500.850	0.158	−31.3	0.0	0.3	67.9	−0.1	0.4	15.9	Fair
53514.962	0.067	−40.8	0.3	0.3	81.0	−0.3	0.4	15.6	Fair
53528.921	0.956	−29.9	0.5	0.3	66.5	−0.3	0.4	16.4	Fair
53536.792	0.021	−39.5	0.1	0.3	79.3	0.0	0.9	14.3	KPNO
53551.964	0.073	−41.1	−0.1	0.3	80.4	−0.7	0.4	15.0	Fair
53609.868	0.907	−19.0	−0.2	0.3	50.3	−0.8	0.4	16.1	Fair
53630.798	0.739	34.6	0.9	0.3	−19.9	−0.2	0.4	. . .	Fair
53646.742	0.896	−16.2	−0.6	0.3	46.5	−0.3	0.4	. . .	Fair
53663.619	0.179	−26.8	0.1	1.0	61.9	−0.3	1.0	12.5	McD
53674.649	0.671	51.2	0.5	0.3	−42.9	−0.2	0.4	16.0	Fair
53691.594	0.964	−32.3	−0.4	1.0	68.4	−0.5	1.0	14.3	McD
53855.930	0.196	−21.9	0.9	0.3	56.5	0.0	0.9	12.9	KPNO
53863.807	0.262	−3.9	0.1	0.3	31.5	0.3	0.4	. . .	Fair
53876.980	0.044	−40.5	0.4	0.3	81.4	0.3	0.4	15.9	Fair
53903.900	0.686	47.4	0.0	0.3	−38.6	−0.3	0.4	15.5	Fair
54002.722	0.056	−41.1	0.1	0.3	81.2	−0.2	0.9	15.3	KPNO
54003.691	0.187	−25.3	−0.2	0.3	59.4	−0.2	0.9	15.5	KPNO
54005.649[b]	0.452	51.0	−0.1	0.3	−43.1	0.2	0.9	. . .	KPNO
54022.734	0.763	26.1	−0.1	0.3	−10.1	−0.4	0.4	. . .	Fair
54220.942	0.579	62.4	0.3	0.3	−58.2	0.0	0.9	16.2	KPNO
54368.628[b]	0.559	62.4	−0.1	0.3	−59.2	−0.5	0.9	. . .	KPNO
54369.710	0.705	43.1	0.3	0.3	−31.7	0.4	0.9	16.4	KPNO
54583.006	0.562	62.1	−0.4	0.3	−58.6	0.1	0.9	. . .	KPNO
54585.986	0.965	−32.3	−0.1	0.3	69.4	0.2	0.9	15.5	KPNO
54644.940[b]	0.941	−26.3	0.9	0.3	62.6	0.1	0.9	. . .	KPNO
54868.012	0.120	−37.7	−0.4	0.3	76.0	−0.2	0.4	15.6	Fair
54947.985	0.940	−26.8	0.1	0.3	62.3	0.2	0.9	15.4	KPNO
55004.900	0.640	56.0	−0.3	0.3	−50.4	0.0	0.9	15.4	KPNO
55041.954	0.653	54.6	0.4	0.3	−47.6	−0.1	0.4	13.7	Fair
55043.779	0.899	−16.4	0.3	0.3	48.8	0.5	0.4	. . .	Fair
55044.774	0.034	−41.2	−0.7	0.3	80.5	0.0	0.4	. . .	Fair
55071.789	0.689	47.2	0.4	0.3	−37.0	0.5	0.4	. . .	Fair
55093.771	0.663	52.5	0.2	0.3	−44.4	0.6	0.9	15.6	KPNO
55095.639	0.916	−21.2	−0.2	0.3	54.4	0.2	0.9	13.9	KPNO
55096.789	0.071	−41.0	0.0	0.3	82.1	0.9	0.4	15.8	Fair
55111.670	0.084	−40.9	−0.4	0.3	80.9	0.4	0.4	16.5	Fair
55138.640	0.733	35.7	0.5	0.3	−22.4	−0.5	0.4	. . .	Fair
55163.625	0.113	−38.3	−0.2	0.3	77.9	0.6	0.4	14.6	Fair
55281.924	0.118	−36.9	0.7	0.3	77.0	0.4	0.4	15.3	Fair
55304.910	0.228	−14.9	−0.5	0.3	45.5	0.3	0.4	. . .	Fair
55314.847	0.572	62.3	0.0	0.3	−59.0	−0.5	0.4	14.1	Fair
55320.936	0.396	38.2	0.6	0.3	−25.2	−0.1	0.4	. . .	Fair

Table 6
(Continued)

Hel. Julian Date (HJD − 2,400,000)	Phase	V_1 (km s^{-1})	$(O-C)_1$ (km s^{-1})	Wt$_1$	V_2 (km s^{-1})	$(O-C)_2$ (km s^{-1})	Wt$_2$	V_3 (km s^{-1})	Source[a]
55340.981	0.108	−38.2	0.5	0.3	77.7	−0.4	0.4	16.1	Fair
55355.937	0.131	−36.4	−0.5	0.3	74.0	−0.2	0.4	15.2	Fair
55361.903	0.938	−27.0	−0.4	0.3	61.9	0.2	0.4	14.2	Fair
55367.911	0.751	30.5	0.5	0.3	−14.8	0.0	0.4	. . .	Fair
55367.932	0.754	28.7	−0.4	0.3	−13.8	−0.2	0.9	. . .	KPNO
55374.803	0.683	48.2	0.2	0.3	−39.1	0.1	0.4	15.6	Fair
55411.935	0.707	42.1	−0.3	0.3	−31.7	−0.2	0.4	15.9	Fair
55459.660	0.164	−30.0	0.2	0.3	66.8	0.2	0.4	16.1	Fair
55463.701	0.710	41.1	−0.4	0.3	−29.7	0.6	0.9	16.4	KPNO
55469.708	0.523	61.8	0.7	0.3	−57.1	−0.3	0.4	14.8	Fair
55478.624	0.729	37.6	1.3	0.3	−23.2	0.2	0.4	. . .	Fair
55481.749	0.152	−32.5	−0.1	0.3	69.4	−0.2	0.4	14.1	Fair
55495.658	0.034	−39.9	0.6	0.3	80.0	−0.5	0.4	15.1	Fair
55505.627	0.382	34.8	0.9	0.3	−19.5	0.5	0.4	. . .	Fair
55516.627	0.871	−7.6	0.6	0.3	36.4	−0.5	0.4	. . .	Fair
55626.002	0.668	51.4	0.1	0.3	−42.8	0.8	0.4	15.3	Fair
55643.961	0.098	−39.5	0.1	0.3	79.5	0.2	0.4	15.4	Fair
55649.919	0.904	−17.3	0.5	0.3	49.6	−0.2	0.4	16.0	Fair
55664.867	0.926	−23.3	0.3	0.3	57.6	−0.1	0.4	14.8	Fair
55669.979	0.617	59.5	0.2	0.3	−54.2	0.1	0.4	13.4	Fair
55677.913	0.691	47.3	1.0	0.3	−36.6	0.3	0.4	. . .	Fair
55680.957	0.103	−39.6	−0.4	0.3	78.3	−0.4	0.9	14.5	KPNO
55684.832	0.627	59.1	1.0	0.3	−52.2	0.6	0.4	16.7	Fair
55694.779	0.973	−32.7	0.8	0.3	71.8	0.8	0.4	14.6	Fair
55698.776	0.513	59.5	−0.8	0.3	−55.8	−0.1	0.4	14.1	Fair
55710.816	0.142	−34.2	−0.1	0.3	72.1	0.2	0.4	15.4	Fair
55718.975	0.246	−8.4	0.6	0.3	38.0	0.1	0.4	. . .	Fair
55725.939	0.188	−25.2	−0.4	0.3	60.2	1.0	0.4	14.5	Fair
55731.939	1.000	−38.1	−0.6	0.3	76.8	0.3	0.9	15.4	KPNO
55732.897	0.130	−36.3	−0.2	0.3	74.3	−0.2	0.9	15.3	KPNO
55732.924	0.133	−35.1	0.4	0.3	72.9	−0.9	0.4	14.9	Fair
55735.933	0.540	61.7	−0.4	0.3	−58.6	−0.5	0.9	. . .	KPNO
55743.877	0.615	59.9	0.4	0.3	−54.8	−0.1	0.4	14.5	Fair
55857.686	0.012	−38.8	0.1	0.3	78.8	0.5	0.4	14.4	Fair
55977.035	0.159	−30.9	0.3	0.3	68.0	0.1	0.4	15.2	Fair
55997.944	0.988	−35.6	0.3	0.3	74.0	−0.2	0.4	14.8	Fair
56023.876	0.496	58.8	0.5	0.3	−53.4	−0.3	0.4	14.8	Fair
56047.820	0.735	35.7	1.1	0.3	−21.2	−0.1	0.4	. . .	Fair
56054.789	0.678	49.9	0.7	0.3	−40.2	0.6	0.4	16.1	Fair
56060.929	0.509	59.4	−0.4	0.3	−55.4	−0.3	0.9	16.2	KPNO
56061.773	0.623	58.8	0.2	0.3	−53.6	−0.1	0.4	14.3	Fair
56061.924	0.643	55.2	−0.6	0.3	−49.8	−0.2	0.9	14.4	KPNO
56067.811	0.440	48.7	0.1	0.3	−40.1	−0.2	0.4	14.4	Fair
56076.731	0.647	55.2	0.0	0.3	−48.6	0.3	0.4	15.2	Fair
56082.769	0.463	52.7	−0.6	0.3	−46.0	0.3	0.4	14.2	Fair
56087.915	0.160	−30.7	0.3	0.3	67.7	0.1	0.4	15.1	Fair
56095.897	0.240	−10.6	0.3	0.3	40.7	0.2	0.4	. . .	Fair
56100.847	0.909	−19.0	0.3	0.3	51.7	−0.2	0.4	15.1	Fair
56126.855	0.428	46.5	0.7	0.3	−35.7	0.5	0.4	15.2	Fair
56169.819	0.240	−10.3	0.4	0.3	40.8	0.6	0.4	. . .	Fair
56196.716	0.879	−11.2	−0.4	0.3	40.6	0.2	0.4	. . .	Fair
56213.685	0.175	−27.2	0.6	0.3	63.6	0.3	0.4	14.3	Fair
56228.657	0.200	−21.2	0.5	0.3	55.1	0.0	0.4	15.2	Fair
56328.034	0.645	55.8	0.3	0.3	−49.1	0.1	0.4	14.4	Fair
56351.012	0.754	29.9	0.8	0.3	−13.6	0.0	0.4	. . .	Fair
56372.966	0.724	37.7	−0.1	0.3	−25.6	−0.2	0.4	. . .	Fair
56389.958	0.023	−39.6	0.2	0.3	79.8	0.3	0.4	15.0	Fair
56400.871	0.499	59.2	0.4	0.3	−53.2	0.5	0.4	. . .	Fair
56414.855	0.391	37.0	0.7	0.3	−23.5	−0.2	0.4	15.2	Fair
56419.828	0.064	−41.0	0.1	0.3	81.0	−0.3	0.4	14.9	Fair
56433.828	0.958	−30.6	0.2	0.3	67.6	0.2	0.4	14.4	Fair

Notes.

[a] McD = McDonald Observatory, Fair = Fairborn Observatory, KPNO = Kitt Peak National Observatory.

[b] Blue wavelength spectrum.

Table 7
Orbital Elements and Related Parameters of 2 Sge

Parameter	Luyten (1936)	This Study
P (days)	7.390	7.3915807 ± 0.0000057
T (HJD)	. . .	2454408.85 ± 0.10
T_0 (JD)	2421047.175 ± 0.24	. . .
e	0.0 (adopted)	0.00613 ± 0.00065
ω (deg)	. . .	158.4 ± 5.1
K_1 (km s^{-1})	52.8 ± 1.0	51.818 ± 0.052
K_2 (km s^{-1})	77.6 ± 8.0	70.031 ± 0.042
γ (km s^{-1})	11.2 ± 0.7	10.950 ± 0.026
$m_1 \sin^3 i$ ($M_\odot$)	. . .	0.7963 ± 0.0011
$m_2 \sin^3 i$ ($M_\odot$)	. . .	0.5892 ± 0.0011
$a_1 \sin i$ (10^6 km)	. . .	5.2668 ± 0.0053
$a_2 \sin i$ (10^6 km)	. . .	7.1179 ± 0.0042
Standard error of an unit weight observation (km s^{-1})	. . .	0.28
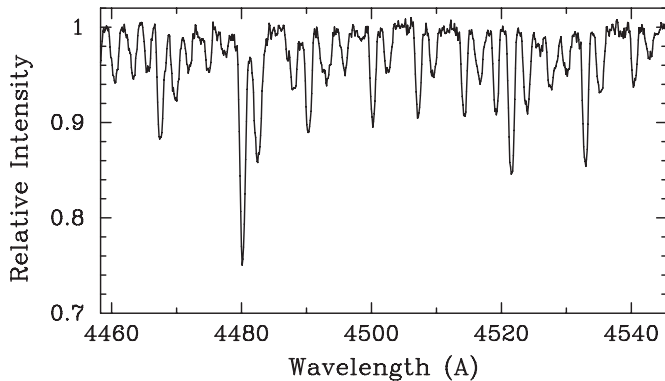
Figure 10. KPNO spectrum of the 4500 Å region of 18 Vul. The strongest feature is the Mg II line at 4481 Å. The more massive primary is the blueshifted component.

Figure 11. Radial velocities of 18 Vul compared with the computed velocity curves. Filled and open symbols represent the primary and secondary, respectively. Circles = Fairborn Observatory, triangles = KPNO, and squares = McDonald Observatory. Zero phase is a time of periastron passage.

4.4. 18 Vul

For 18 Vul, 62 of our 75 spectra showing double lines were obtained at Fairborn Observatory between 2004 and 2013. Of the remaining spectra, acquired from 2005 through 2008, 11 are from KPNO and two from McDonald Observatory. A KPNO spectrum of 18 Vul in the 4500 Å region is shown in Figure 10. Clearly visible are the moderate but still relatively low rotational broadening and the line strength difference between the two components. All our new radial velocity observations are given in Table 8.

We first obtained four orbital solutions, two for the primary and two for the secondary. Because of the extensive number of Fairborn velocities, those data were analyzed first. Separate orbital solutions result in eccentricities of 0.018 ± 0.002 and 0.025 ± 0.005 for the primary and secondary, respectively. Following the precepts of Lucy & Sweeney (1971), we conclude that the orbit is eccentric. However, we note that the longitude of periastron, which for the two solutions should differ by 180°, has a difference of just 43°. Reasons for this apparent discrepancy include the greater difficulty in measuring precise velocities of the broader lined secondary and/or the δ Scuti pulsation.

Because there are just two observations from McDonald Observatory, we added them to the KPNO velocity set and then determined orbital solutions for the two components with that combined data. The variances of the four solutions resulted in weights of 1.0, 0.3, and 0.3 for the primary velocities from Fairborn, KPNO, and McDonald, respectively. For the secondary, the weights were 0.2, 0.05, and 0.05 for the same
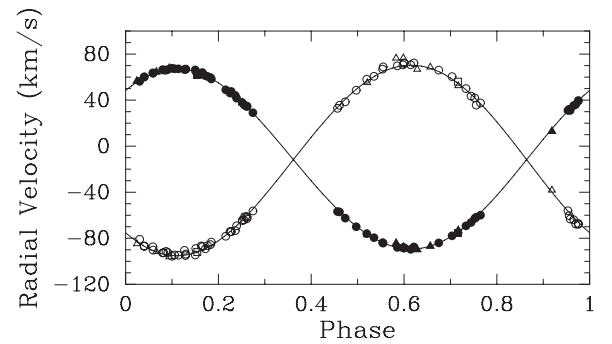
three respective observatories. The center-of-mass velocities of the four data sets agree to within 2.0 km s^{-1} with the 1σ uncertainties in the individual values nearly overlapping. The difference between the center-of-mass velocities for the Fairborn primary and secondary velocities is only 0.4 km s^{-1}. Thus, we combined all our data into a simultaneous solution for both components, which produced an orbital period of 9.31408 days.

The only other significant set of radial velocities is that of Harper (1918), which were determined from photographic plates obtained at the Dominion Observatory in Ottawa. The standard deviation per plate of the primary velocity is 7.2 km s^{-1}, resulting in such low weights that they do not significantly improve the value of the period. Thus, in Table 9 we present the orbital elements from our velocities only. Our primary and secondary velocities are compared with the computed velocity curves in Figure 11. In that plot, zero phase is a time of periastron passage. In Figure 12 the velocity residuals of the two components are plotted versus phase. Compared with the results of our other three systems, the residuals for both components of 18 Vul are much larger. This is primarily due to the substantially greater line broadening of the two components, but may also result from pulsation in one or both components.

Harper (1918) did not provide uncertainties for his derived orbital elements, and so in Table 9 we compare our results to the reanalysis of Harper's velocities that was computed by Luyten (1936). The uncertainty of our period and semi-amplitudes is significantly improved. Our semi-amplitudes are both smaller than those of Harper's with that for the secondary being reduced

13

Table 8
Radial Velocities of 18 Vul

Hel. Julian Date (HJD − 2,400,000)	Phase	V_1 (km s^{-1})	$(O − C)_1$ (km s^{-1})	Wt$_1$	V_2 (km s^{-1})	$(O − C)_2$ (km s^{-1})	Wt$_2$	Source[a]
53311.719	0.150	66.3	1.5	1.0	−94.5	−1.9	0.20	Fair
53312.695	0.255	36.1	−0.6	1.0	−64.1	−1.2	0.20	Fair
53354.614	0.755	−61.7	−0.3	1.0	35.7	−5.1	0.20	Fair
53638.655[b]	0.251	37.7	−0.4	0.3	−61.6	2.7	0.05	KPNO
53689.554[b]	0.716	−75.0	−0.5	0.3	56.0	1.3	0.05	McD
53855.967	0.583	−84.3	3.5	0.3	76.5	7.8	0.05	KPNO
54005.678[b]	0.657	−86.9	−0.1	0.3	68.7	1.0	0.05	KPNO
54047.571	0.154	62.0	−2.3	0.3	−92.0	0.0	0.05	McD
54223.976	0.094	67.7	0.8	0.3	−96.1	−1.3	0.05	KPNO
54265.931	0.598	−87.7	1.2	0.3	76.6	6.7	0.05	KPNO
54269.897	0.024	56.5	0.9	0.3	−84.8	−1.9	0.05	KPNO
54367.663	0.521	−76.7	−0.2	0.3	55.2	−1.6	0.05	KPNO
54368.665[b]	0.628	−89.8	−0.7	0.3	66.8	−3.3	0.05	KPNO
54408.625	0.919	12.9	−2.2	0.3	−38.2	1.8	0.05	KPNO
54586.967[b]	0.066	64.4	0.2	0.3	−91.6	0.3	0.05	KPNO
54732.738	0.717	−73.2	1.1	0.3	52.5	−1.9	0.05	KPNO
55275.966	0.040	60.3	0.8	1.0	−86.7	0.3	0.20	Fair
55293.899	0.966	35.3	−0.5	1.0	−63.9	−2.0	0.20	Fair
55314.857	0.216	49.0	−1.4	1.0	−78.2	−0.8	0.20	Fair
55331.848	0.040	60.0	0.6	1.0	−87.0	−0.1	0.20	Fair
55341.772	0.105	67.3	0.0	1.0	−94.5	0.7	0.20	Fair
55377.817	0.975	39.1	−0.5	1.0	−67.9	−1.9	0.20	Fair
55401.833	0.554	−83.8	0.0	1.0	66.9	2.4	0.20	Fair
55412.820	0.733	−69.2	−0.1	1.0	50.0	1.0	0.20	Fair
55459.683	0.765	−59.9	−2.2	1.0	37.5	0.6	0.20	Fair
55513.613	0.555	−84.2	−0.2	1.0	68.9	4.2	0.20	Fair
55554.602	0.956	32.1	0.4	1.0	−60.3	−2.7	0.20	Fair
55631.962	0.262	34.5	0.4	1.0	−63.0	−2.9	0.20	Fair
55640.959	0.227	47.6	0.9	1.0	−74.4	−1.0	0.20	Fair
55648.919	0.082	66.1	0.1	1.0	−92.6	1.3	0.20	Fair
55653.941	0.621	−87.5	1.8	1.0	72.3	2.0	0.20	Fair
55662.923	0.586	−87.9	0.1	1.0	69.8	0.8	0.20	Fair
55667.985	0.129	67.0	0.2	1.0	−95.0	−0.4	0.20	Fair
55675.871	0.976	39.7	−0.1	1.0	−67.2	−1.1	0.20	Fair
55680.936	0.520	−76.0	0.1	1.0	58.1	1.7	0.20	Fair
55704.782	0.080	66.5	0.7	1.0	−92.7	0.9	0.20	Fair
55732.910	0.100	67.7	0.6	1.0	−95.6	−0.6	0.20	Fair
55844.809	0.114	67.2	−0.1	1.0	−94.7	0.5	0.20	Fair
55892.660	0.251	37.9	−0.3	1.0	−64.5	−0.1	0.20	Fair
55967.034	0.236	44.1	0.5	1.0	−73.4	−3.2	0.20	Fair
55989.028	0.598	−88.2	0.7	1.0	70.6	0.7	0.20	Fair
56011.950	0.059	63.7	0.7	1.0	−87.4	3.3	0.20	Fair
56012.922	0.163	62.5	−0.5	1.0	−86.7	3.9	0.20	Fair
56040.885	0.165	64.0	1.4	1.0	−87.4	2.8	0.20	Fair
56058.821	0.091	66.6	−0.1	1.0	−92.4	2.2	0.20	Fair
56064.907	0.744	−66.3	−0.9	1.0	43.5	−1.6	0.20	Fair
56068.889	0.172	61.2	−0.2	1.0	−89.1	−0.1	0.20	Fair
56077.784	0.127	66.6	−0.3	1.0	−90.5	4.3	0.20	Fair
56086.727	0.087	66.0	−0.4	1.0	−91.4	2.9	0.20	Fair
56097.785	0.274	29.1	0.3	1.0	−56.3	−1.7	0.20	Fair
56100.816	0.600	−88.6	0.4	1.0	72.3	2.3	0.20	Fair
56101.783	0.704	−77.9	0.0	1.0	60.4	2.1	0.20	Fair
56227.724	0.225	46.2	−1.3	1.0	−74.2	0.0	0.20	Fair
56236.646	0.183	59.6	0.5	1.0	−85.5	1.1	0.20	Fair
56274.635	0.262	34.8	0.8	1.0	−61.5	−1.4	0.20	Fair
56342.025	0.497	−70.0	−0.5	1.0	48.6	−0.8	0.20	Fair
56352.994	0.675	−84.0	0.1	1.0	66.1	1.3	0.20	Fair
56374.933	0.030	56.3	−0.8	1.0	−80.9	3.6	0.20	Fair
56392.890	0.958	31.1	−1.6	1.0	−63.3	−4.7	0.20	Fair
56406.888	0.461	−57.1	−0.5	1.0	35.5	−0.3	0.20	Fair
56416.895	0.535	−79.5	0.5	1.0	60.7	0.2	0.20	Fair
56418.917	0.752	−62.8	−0.3	1.0	41.9	−0.1	0.20	Fair
56420.787	0.953	31.1	0.5	1.0	−56.1	0.4	0.20	Fair
56420.944	0.970	36.2	−1.4	1.0	−67.7	−3.9	0.20	Fair

Table 8
(Continued)

Hel. Julian Date (HJD − 2,400,000)	Phase	V_1 (km s^{-1})	$(O-C)_1$ (km s^{-1})	Wt$_1$	V_2 (km s^{-1})	$(O-C)_2$ (km s^{-1})	Wt$_2$	Source[a]
56421.773	0.059	63.3	0.2	1.0	−90.2	0.6	0.20	Fair
56422.869	0.177	60.6	0.2	1.0	−86.4	1.6	0.20	Fair
56422.944	0.185	58.3	−0.4	1.0	−83.3	2.8	0.20	Fair
56426.816	0.601	−88.2	0.8	1.0	72.0	2.0	0.20	Fair
56426.944	0.614	−89.6	−0.3	1.0	70.7	0.3	0.20	Fair
56431.747	0.130	66.8	0.1	1.0	−93.7	0.9	0.20	Fair
56431.945	0.151	64.8	0.1	1.0	−88.9	3.6	0.20	Fair
56432.765	0.239	41.7	−0.9	1.0	−69.2	−0.1	0.20	Fair
56432.945	0.259	35.0	−0.3	1.0	−61.1	0.3	0.20	Fair
56434.790	0.457	−56.8	−1.9	1.0	32.9	−1.1	0.20	Fair
56434.945	0.473	−62.5	−1.2	1.0	38.5	−2.2	0.20	Fair

Notes.
[a] Fair = Fairborn Observatory, KPNO = Kitt Peak National Observatory, and McD = McDonald Observatory.
[b] Blue wavelength spectrum.

Table 9
Orbital Elements and Related Parameters of 18 Vul

Parameter	Luyten (1936)	This Study
P (days)	9.316	9.314077 ± 0.000039
T (HJD)	. . .	2454875.09 ± 0.25
T_0 (JD)	2421103.17 ± 0.03	. . .
e	0.0 (adopted)	0.0116 ± 0.0019
ω (deg)	. . .	319.4 ± 0.97
K_1 (km s^{-1})	78.5 ± 1.4	78.33 ± 0.13
K_2 (km s^{-1})	86.3 ± 1.4	82.80 ± 0.29
γ (km s^{-1})	-13.0 ± 1.0	-11.70 ± 0.11
$m_1 \sin^3 i$ ($M_\odot$)	. . .	2.074 ± 0.014
$m_2 \sin^3 i$ ($M_\odot$)	. . .	1.9622 ± 0.0090
$a_1 \sin i$ (10^6 km)	. . .	10.032 ± 0.017
$a_2 \sin i$ (10^6 km)	. . .	10.604 ± 0.037
Standard error of an unit weight observation (km s^{-1})	. . .	0.86
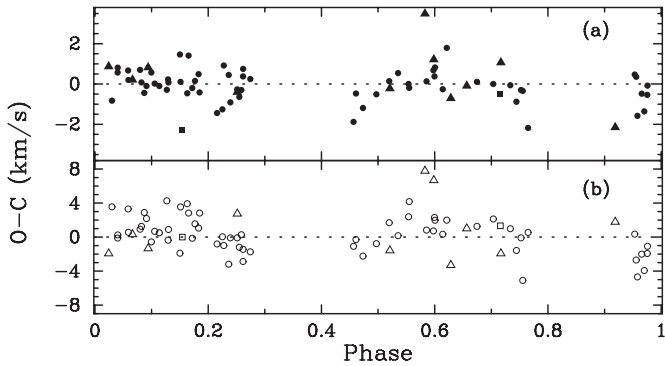
Figure 12. 18 Vul radial velocity residuals vs. orbital phase. Panel (a) shows residuals of the primary, while panel (b) is of the secondary. Circles = Fairborn Observatory, triangles = KPNO, and squares = McDonald Observatory. Zero phase is a time of periastron passage.

by 4%. While this results in smaller minimum masses, both stars still have minimum values that are about 2 $M_\odot$.

5. SPECTRAL TYPES AND MAGNITUDE DIFFERENCE

Strassmeier & Fekel (1990) identified several luminosity-sensitive and temperature-sensitive line ratios in the 6430–6465 Å region. They employed those critical line ratios and the general appearance of the spectrum as spectral-type criteria. For our A-star binaries we have examined the gen-

eral appearance of our KPNO spectra in both the 4500 Å and 6430 Å regions to determine spectral classes. However, the obvious abundance peculiarities in many of the components of our A-star systems make normal spectral classification very difficult in our two limited 84 Å regions. Also, in those two regions the line ratios of A and F spectral class stars have little sensitivity to luminosity. Thus, it is necessary to determine the luminosity class by computing the absolute visual magnitude with the *Hipparcos* parallax. Those magnitudes, converted to luminosities, and the adopted temperatures of the stars are then compared to evolutionary tracks. Because such luminosity classes are not assigned from the appearance of the spectra, we have used words such as dwarf or subgiant to describe the luminosity class rather than using Roman numerals.

The comparison spectra for our binaries are mostly slowly rotating A stars from the list of Abt & Morrell (1995) plus a few F and G stars from Fekel (1997). Those spectra were acquired at KPNO with the same telescope, spectrograph, and detector as our binary star spectra. In an attempt to reproduce the binary spectra, various comparison-star combinations were rotationally broadened when necessary, shifted in radial velocity to mimic the separation of the two components, appropriately weighted, and added together with a computer program developed by Huenemoerder & Barden (1984) and Barden (1985).

From the equivalent widths of line pairs, we determined the continuum intensity ratio of the binary components at 4500 Å in our KPNO spectra. The continuum intensity ratio at 5700 Å is

from our Fairborn Observatory spectra that were measured with the A-star line list, while that same ratio at 6000 Å is from our solar-type star line list. The continuum intensity ratio is equal to the luminosity ratio and converted to a magnitude difference if the stars have the same or very similar spectral types. If, on the other hand, the components are main-sequence stars of very different spectral types, then the lines of the secondary are intrinsically significantly stronger than those of the primary. In that case, the continuum intensity ratio becomes a minimum magnitude difference. Abundance peculiarities, such as those in Am stars, make any such magnitude difference even more uncertain.

Abt & Morrell (1995) stated that based on their hydrogen lines, classical Am stars have spectral classes ranging from A4 to F1. The Am stars are identified as peculiar because relative to the hydrogen classification, various elements including Fe and Sr are stronger than expected, leading to a later spectral class, and other elements like Ca and Sc have weaker lines than expected, resulting in an earlier spectral class (Abt & Morrell 1995). Our limited regions around 4500 Å and 6430 Å contain no hydrogen lines. In addition, the overabundance and underabundance peculiarities vary from star to star. Thus, the spectral class analysis of our binary systems has met with limited success especially for those components that are Am stars.

5.1. HR 1528

As noted by Bidelman (Abt & Bidelman 1969), HR 1528 has pronounced Am star characteristics. Abt & Morrell (1995) classified the combined spectrum of HR 1528 as an Am star with A7, F0, and F2 spectral classes for its Ca K, hydrogen, and metal lines, respectively. Thus, because HR 1528 is an Am star, our analysis of its spectrum is limited. Comparison with reference stars indicates that the Fe I lines at red wavelengths are similar in strength to those of HR 5075 (F2 V; Abt & Morrell 1995), while the $B - V$ color indicates a spectral type of A8/9 V.

From our Fairborn observations, the secondary to primary line strength ratio at ~6000 Å is 2.37. However, the Am star nature of the primary with its strengthened Fe lines makes this value suspect. In addition, such a large magnitude difference between the primary and the secondary means that the lines of the secondary are very weak. Thus, the secondary spectral class is not well determined. From the secondary to primary mass ratio of 0.66 and the canonical properties tables of Gray (1992), we estimate a V magnitude difference of 2.1 ± 0.4 (Gray 1992) suggesting that the spectral type of the secondary is a late-F or early-G dwarf. The evolutionary track comparison discussed in Section 6.1 indicates that both components are main-sequence stars.

5.2. HR 6993

Although its sharp lines would suggest that HR 6993 is an early-type Am star, Cowley et al. (1969), Floquet (1975), and Levato & Abt (1978) classified the combined spectrum as a normal A2 V star. Based on a 13 A mm^{-1} spectrogram that resolved the narrow lines of the binary, Geary & Abt (1970) concluded that while the primary has a normal spectrum, the secondary appears to be an Am star.

Both our blue and red wavelength KPNO spectra show that most of the line pairs are similar in strength. HR 4378 (A2 Vs; Abt & Morrell 1995) provides a reasonably good fit to the spectrum of HR 6993 at both blue and red wavelengths, but the Ca I lines of the secondary are indeed weaker than expected from the general fit.

At 5700 Å the continuum intensity ratio of the secondary to the primary is 0.705, which results in a continuum magnitude difference of 0.4 ± 0.1, while at 4500 Å the intensity ratio is 0.764, resulting in a continuum magnitude difference of 0.3 ± 0.1. This value is similar to that of Petrie (1950), who analyzed a blue photographic plate and found a difference of 0.16 ± 0.06 at a mean wavelength of 4450 Å from just three line pairs.

The secondary has a very similar spectral class to the primary, and so we adopt a V magnitude difference of 0.4 ± 0.1. As discussed in Section 6.2, visual magnitudes from the reanalyzed *Hipparcos* parallax (van Leeuwen 2007) indicate that both components are on the main sequence.

5.3. 2 Sge

The difficulty of identifying peculiarities in early-type A stars from low-dispersion classification spectra is exemplified by 2 Sge. Cowley et al. (1969) indicated that 2 Sge is a mild metallic-lined A star, and Bidelman (Abt & Bidelman 1969) concluded that it is a probable Am star, while Bertaud (1970) classified it as a full-fledged Am star with its Ca K line being A2 and its metal lines A7. On the other hand, other classifiers have found no spectrum peculiarities. Levato (1975) assigned a spectral type of A2 III–IV, while Abt & Morrell (1995) classified its spectral type as A1 III.

Stickland (1973) performed a spectroscopic analysis that indicated an overabundance of Fe and an underabundance of Sc in both components as expected for Am stars. Our examination of the 6430 Å region confirms that both short-period components have an overabundance of Fe while Ca appears to be underabundant. Very weak lines of the close visual secondary, discovered by the *Hipparcos* team (Perryman et al. 1997), are also visible in this wavelength region (Figure 6).

At 4500 Å the continuum intensity ratio is 0.336, which converts to a magnitude difference of 1.2 ± 0.1. For lines centered at 5700 Å, an intensity ratio of 0.479 produces a 0.8 ± 0.1 mag difference. These values assume that the Fe surface abundances of the two stars are the same, which, because both components are Am stars, is not necessarily the case. The combined $B - V$ value and the mass ratio compared with canonical values in Table B1 of Gray (1992) suggest spectral classes of A2 and A7 and a V magnitude difference of 1.0 ± 0.2, which we adopt. From our discussion in Section 6.3, both components appear to be main-sequence stars.

5.4. 18 Vul

Spectral types of 18 Vul include A1 IV (Svolopoulos 1961), A2 IV (Abt & Morrell 1995), A3 V (Cowley et al. 1969), and A3 III (Osawa 1959). Bidelman (Abt & Bidelman 1969) concluded that its spectrum was that of a normal A star with no peculiarities.

Our blue and red wavelength spectra show that the components are somewhat similar in strength with the weaker lined secondary rotating more rapidly. Thus, we compared its spectrum with the reference stars HR 4378 (A2 Vs; Abt & Morrell 1995) and 68 Tau (A2 IV; Abt & Morrell 1995). An abundance analysis by Pintado & Adelman (2003) has shown that 68 Tau is an early-type Am star with stronger Fe lines and weaker Ca lines than expected for its hydrogen spectral type. In general, the Fe lines of 18 Vul are fitted better by 68 Tau than by HR 4378. However, the Ca lines of 18 Vul are similar in strength to HR 4378 and significantly stronger than those of 68 Tau. Thus, we find no obvious abundance peculiarities.

At 5700 Å the continuum intensity ratio of the secondary to the primary is 0.601, which results in a continuum magnitude

Table 10
Derived Properties of the Binary Components

Parameter	HR 1528	HR 6993	2 Sge	18 Vul
V_1 (mag)	5.99 ± 0.05	6.33 ± 0.10	6.63 ± 0.20	6.00 ± 0.10
V_2 (mag)	8.09 ± 0.40	6.73 ± 0.10	7.63 ± 0.20	6.60 ± 0.10
L_1 ($L_\odot$)	21.3 ± 2.0	60.5 ± 8.5	22.6 ± 4.9	51.6 ± 6.0
L_2 ($L_\odot$)	3.3 ± 1.2	41.9 ± 5.9	8.4 ± 1.8	31.1 ± 3.6
R_1 ($R_\odot$)	2.7 ± 0.2	3.4 ± 0.3	2.0 ± 0.3	3.5 ± 0.3
R_2 ($R_\odot$)	1.7 ± 0.3	2.8 ± 0.2	1.6 ± 0.2	2.4 ± 0.2
M_1[a] ($M_\odot$)	1.95	2.5	2.08	2.4
M_2[a] ($M_\odot$)	1.2:[b]	2.35	1.67	2.2

Notes.
[a] Masses are estimated from evolutionary tracks in Figure 13.
[b] The colon indicates a very uncertain value.

difference of 0.55 ± 0.1, while at 4500 Å the intensity ratio is 0.535, resulting in a continuum magnitude difference of 0.7 ± 0.1. The spectral classes for the two stars appear to be similar, and so we adopt a V magnitude difference of 0.6 ± 0.1. From our discussion in Section 6.4, we classify the primary and secondary as dwarf stars.

6. BASIC PROPERTIES

6.1. HR 1528

To determine the basic properties of HR 1528, we use the Stefan–Boltzmann law. We begin by adopting a V mag of 5.84 and a $B - V$ color of 0.250 mag from the *Hipparcos* catalog (Perryman et al. 1997). With our adopted V magnitude difference of 2.1 ± 0.4, the individual V magnitudes are 5.99 and 8.09 for the primary and secondary, respectively. The new *Hipparcos* parallax reduction by van Leeuwen (2007) produces a value of 11.94 ± 0.49 mas and corresponds to a distance of 83.8 ± 3.5 pc. At such a distance we assume that the interstellar extinction is negligible. The resulting absolute magnitudes are $M_V = 1.38 \pm 0.10$ mag and $M_V = 3.48 \pm 0.40$ mag for the primary and secondary, respectively. The uncertainty in the luminosity ratio has a much greater effect on the secondary than the primary. Given the large magnitude difference, the $B - V$ color of the primary will be only slightly smaller than the combined value, and we adopt a value of 0.23 for it. The minimum mass of the secondary indicates that it may well be a late-F or early-G star, a result consistent with the adopted magnitude difference, and so we use 0.56 for its $B - V$. For the two components, the effective temperatures and bolometric corrections come from Table 3 of Flower (1996). From spectral type and temperature calibration uncertainties, we estimate effective temperature uncertainties of ± 200 K for both components. Then our luminosities of the primary and secondary are $L_1 = 21.3 \pm 2.0\,L_\odot$ and $L_2 = 3.3 \pm 1.2\,L_\odot$, respectively, while the radii are $R_1 = 2.7 \pm 0.2\,R_\odot$ and $R_2 = 1.7 \pm 0.3\,R_\odot$, respectively. These derived basic parameters are listed in Table 10.

Our estimated effective temperatures and luminosities for the components of HR 1528 are compared with the solar-abundance evolutionary tracks of Girardi et al. (2000) in Figure 13. Although the surface enhancement of Fe and other metals may make Am stars such as the primary of HR 1528 appear to be metal rich, that component is still on the main sequence. When compared to those of solar composition, metal-rich tracks for the same masses (Girardi et al. 2000) are shifted to cooler temperatures and lower luminosities. This results in a position for the Am star component that is closer to the zero-age main sequence but of higher mass. The much lower mass
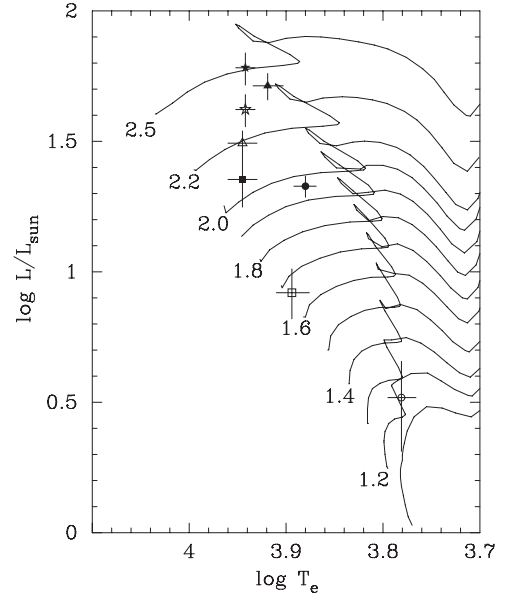

Figure 13. Positions of the components of HR 1528 (circles), HR 6993 (stars), 2 Sge (squares), and 18 Vul (triangles) compared with the 1.1–2.5 $M_\odot$ solar-abundance evolutionary tracks of Girardi et al. (2000). The more massive star in each system corresponds to the filled symbol. Our estimated uncertainties are shown.

secondary is also a main-sequence star. Masses estimated from the evolutionary tracks are given in Table 10.

6.2. HR 6993

As we did for HR 1528, we estimate the basic properties of HR 6993 using the Stefan–Boltzmann law. We first adopt a V mag of 5.76 and a $B - V$ color of 0.067 mag from the *Hipparcos* catalog (Perryman et al. 1997). With a ΔV of 0.4 ± 0.1 mag, the V magnitudes of the primary and secondary are 6.33 and 6.73 mag, respectively. The system parallax of 6.23 ± 0.033 mas (van Leeuwen 2007) results in a distance of 160.5 ± 8.6 pc. Although at this distance there might be a modest amount of reddening, the spectral type is consistent with the $B - V$ color and Hβ value (Stokes 1972; Crawford 1979), and so we assume that there is no reddening for this star system. The components' absolute magnitudes are $M_V = 0.30 \pm 0.15$ and $M_V = 0.70 \pm 0.15$ for the primary and secondary, respectively. Table 3 of Flower (1996) then provides the bolometric corrections and effective temperatures that we adopt for the stars. The effective temperature uncertainties are estimated to be ± 200 K for both components. We then determine luminosities of $L_1 = 60.5 \pm 8.5\,L_\odot$ and $L_2 = 41.9 \pm 5.9\,L_\odot$ and radii of $R_1 = 3.4 \pm 0.3\,R_\odot$ and $R_2 = 2.8 \pm 0.2\,R_\odot$ for the primary and secondary, respectively. These derived basic parameters are given in Table 10.

Our estimated temperatures and luminosities for the two stars are plotted in a Hertzsprung–Russell (H-R) diagram (Figure 13) and compared to the solar-abundance evolutionary tracks of Girardi et al. (2000). The positions of the two components in the H-R diagram indicate that both stars are dwarfs. Masses estimated from the evolutionary tracks are listed in Table 10.

6.3. 2 Sge

From the *Hipparcos* catalog (Perryman et al. 1997), the V magnitude and $B - V$ color of the 2 Sge system are 6.27 and 0.075, respectively. With the 1.0 ± 0.2 magnitude difference adopted in Section 5.3, the apparent V magnitudes are 6.63 and

7.63 for the short-period primary and secondary, respectively. The *Hipparcos* parallax reduction by van Leeuwen (2007) results in a value of 8.92 ± 0.52 mas and corresponds to a distance of 112.1 ± 6.6 pc. At such a distance we assume that the interstellar extinction is negligible. The apparent magnitudes and parallax then result in absolute magnitudes M_V of 1.38 ± 0.24 and 2.38 ± 0.24 for the primary and secondary, respectively. From Johnson (1966) we assume $B - V$ colors of 0.06 and 0.19 for the two components, respectively. Table 3 of Flower (1996) then provides the bolometric corrections and effective temperatures that we adopt for the stars. The effective temperature uncertainties are estimated to be ± 300 K for both components. The resulting luminosities are $L_1 = 22.6 \pm 4.9 \, L_\odot$ and $L_2 = 8.4 \pm 1.8 \, L_\odot$, and the radii are $R_1 = 2.0 \pm 0.3 \, R_\odot$ and $R_2 = 1.6 \pm 0.2 \, R_\odot$ for the primary and secondary, respectively. These derived basic properties are summarized in Table 10.

In Figure 13 we plot our estimated temperatures and luminosities for the short-period components of 2 Sge where those points are compared to the solar-abundance evolutionary tracks of Girardi et al. (2000). Once again, both stars appear to be dwarfs. Masses estimated from the evolutionary tracks are given in Table 10.

6.4. 18 Vul

For the 18 Vul system, we adopt a *V* magnitude and $B - V$ color of 5.51 and 0.087, respectively (Perryman et al. 1997). Using our *V* magnitude difference of 0.6 ± 0.1, we compute individual apparent *V* magnitudes of 6.00 and 6.60. The new reduction of the *Hipparcos* parallax produces a value of 7.70 ± 0.27 mas (van Leeuwen 2007), which corresponds to a distance of 129.9 ± 4.6 pc. At such a distance, there may be a slight amount of interstellar extinction. However, the $B - V$ color and spectral type are consistent, so we have not included any reddening. We then combine the apparent magnitudes and the parallax to obtain absolute magnitudes $M_V = 0.43 \pm 0.13$ and $M_V = 1.03 \pm 0.13$ for the primary and secondary, respectively. The difference in spectral class between the two components is not large, perhaps a couple subclasses at most. Thus, from Johnson (1966) we assume $B - V$ colors of 0.12 and 0.06 for the primary and secondary, respectively. We then use Table 3 of Flower (1996) to obtain the bolometric corrections and effective temperatures of the two components, where the effective temperature uncertainty is estimated to be ± 300 K. The resulting luminosities of the primary and secondary are $L_1 = 51.6 \pm 6.0 \, L_\odot$ and $L_2 = 31.1 \pm 3.6 \, L_\odot$, respectively, while the radii are $R_1 = 3.5 \pm 0.3 \, R_\odot$ and $R_2 = 2.4 \pm 0.2 \, R_\odot$, respectively. These basic parameters are listed in Table 10.

Our temperatures and luminosities of the 18 Vul components are compared with the solar-abundance evolutionary tracks of Girardi et al. (2000) in Figure 13. Both stars are on the main sequence. Masses estimated from the evolutionary tracks are also given in Table 10.

7. CIRCULARIZATION AND SYNCHRONIZATION

Zahn (1977) and Tassoul & Tassoul (1992) have produced very different theories for the way that binary orbits become circularized and binary components obtain rotational synchronization. Although their theories predict very different absolute timescales, they both lead to the conclusion that rotational synchronization occurs before orbital circularization. In an observational survey, Matthews & Mathieu (1992) looked at 62 spectroscopic binaries with A-type primaries and periods less

than 100 days. Circular or nearly circular orbits occurred for all the systems that have orbital periods $\lesssim 3$ days. However, even binaries with somewhat longer periods from 3 to 10 days often have circular orbits. HR 1528, 2 Sge, and 18 Vul with periods of 7.1, 7.4, and 9.3 days, respectively, have circular or nearly circular orbits. HR 6993 with its longer 14.7 day period has a moderate eccentricity of 0.25. Thus, the eccentricities of the four systems are consistent with the survey results of Matthews & Mathieu (1992).

In an eccentric orbit, Hut (1981) has shown that the rotational angular velocity of a star will tend to synchronize with that of the orbital motion at periastron, a condition called pseudosynchronous rotation. With Equation (42) of Hut (1981) we compute a pseudosynchronous rotation period of 10.66 days for HR 6993.

To help in assessing component synchronization or pseudosynchronization in our four short-period binaries, we have determined projected rotational velocities of the components from our KPNO red wavelength spectra with the procedure of Fekel (1997). For A-type stars, the measured line broadening was converted to a $v \sin i$ value. For stars with later spectral classes, macroturbulent broadening has been taken into account. Following Fekel (1997) for late-F and G stars, a value of $3 \, \mathrm{km \, s^{-1}}$ was used.

To convert the $v \sin i$ values into equatorial rotational velocities, we assume, as is generally done, that the axes of the orbital and rotational planes are parallel. If that is the case, then the two inclinations are equal, and we can adopt the orbital inclination as the rotational inclination.

7.1. HR 1528

To determine whether the components of HR 1528 are rotating synchronously, we first compute equatorial velocities from our projected rotational velocities. We then compare them with the predicted synchronous velocities. For the primary of HR 1528, our $v \sin i$ value is $10.3 \pm 1.0 \, \mathrm{km \, s^{-1}}$. Because of the secondary's weak lines, its value of $7.5 \pm 2.0 \, \mathrm{km \, s^{-1}}$ has a greater uncertainty than that of the primary. From our comparison with the solar-abundance evolutionary tracks we adopt a mass of $1.95 \, M_\odot$ for the primary (Figure 13). That mass combined with its $m \sin^3 i$ value (Table 3) results in an orbital inclination of $66°$. Adopting that inclination produces rotational velocities of 11.3 and $8.2 \, \mathrm{km \, s^{-1}}$ for the primary and secondary, respectively. With our computed radii from the Stefan–Boltzmann law the synchronous rotational velocities are 19.4 and $12.2 \, \mathrm{km \, s^{-1}}$ for the primary and secondary. The Am star primary is certainly rotating much more slowly than its synchronous value, while on the face of it the late-F or early-G secondary is as well, although the large relative uncertainty, estimated for both its $v \sin i$ and especially its radius, makes synchronous rotation a possibility. For example, a radius of $1.2 \, R_\odot$, appropriate for a late-F dwarf, results in a predicted synchronous rotational velocity of $8.6 \, \mathrm{km \, s^{-1}}$, a value in good agreement with our observed result. In Table 11 we have summarized the observed and predicted rotational velocities.

7.2. HR 6993

To determine if the components of HR 6993 are pseudosynchronously rotating, we initially compute their projected rotational velocities. From our KPNO spectra we determined $v \sin i$ values of 5.6 ± 1.0 and $5.9 \pm 1.0 \, \mathrm{km \, s^{-1}}$ for the primary and secondary, respectively. With our previously computed pseudosynchronous rotation period of 10.66 days and the radii from the

Table 11
Observed and Predicted Synchronous Rotational Velocities

Parameter	HR 1528	HR 6993	2 Sge	18 Vul
$v_1 \sin i$ (km s^{-1})	10.3 ± 1.0	5.6 ± 1.0	9.4 ± 1.0	42.0 ± 2.0
$v_2 \sin i$ (km s^{-1})	7.5 ± 2.0	5.9 ± 1.0	9.8 ± 1.0	51.0 ± 3.0
v_1 (km s^{-1})	11.3 ($i = 66°$)	11.2 ($i = 30°$)	12.9 ($i = 47°$)	44.2 ($i = 72°$)
v_2 (km s^{-1})	8.2 ($i = 66°$)	11.8 ($i = 30°$)	13.4 ($i = 47°$)	53.6 ($i = 72°$)
v_1(sync) (km s^{-1})	19.4	16.1[a]	13.7	19.0
v_2(sync) (km s^{-1})	12.2	13.3[a]	11.0	13.0

Note. [a] Predicted pseudosynchronous rotational velocity.

Stefan–Boltzmann law, the pseudosynchronous rotational velocities for the primary and secondary are 16.1 and 13.3 km s^{-1}, respectively. The minimum masses from our orbital solution are about 0.3 $M_\odot$, the smallest values of our four systems. If we adopt a mass of 2.5 $M_\odot$ for the primary from the comparison with solar-abundance evolutionary tracks in Figure 13, we obtain an orbital inclination of 30°. Assuming that the orbital and rotational inclinations are equal, then our $v \sin i$ values are doubled. This results in equatorial rotational velocities of 11.2 and 11.8 km s^{-1} for the primary and secondary, respectively. The value of the primary is still significantly less than its computed pseudosynchronous rotational velocity. While the value for the secondary is also less than its pseudosynchronous velocity, the uncertainties of the various quantities make it possible that it is rotating pseudosynchronously. The observed and predicted rotational velocities are compared in Table 11.

7.3. 2 Sge

The orbit for the short-period pair of 2 Sge has an eccentricity of less than 0.01, and so we simply examine the case for synchronous rotation of the components. Their projected rotational velocities from our KPNO spectra are 9.4 ± 1.0 and 9.8 ± 1.0 km s^{-1} for the primary and secondary, respectively. With radii from the Stefan–Boltzmann law we determine synchronous equatorial rotational velocities of 13.7 and 11.0 km s^{-1}. Again, comparing the minimum mass of the primary with its mass of 2.08 $M_\odot$ estimated from evolutionary tracks (Figure 13), we obtain an inclination of 47°. Adopting this value increases the $v \sin i$ results to rotational velocities of 12.9 and 13.4 km s^{-1} for the primary and secondary, respectively. Thus, the primary of the short-period binary appears to be rotating synchronously. The secondary may be rotating faster than synchronous, although the predicted synchronous value and the observed value are uncertain enough that the secondary also may be synchronously rotating. We list the observed and predicted rotational velocities in Table 11.

For completeness sake, we note that the $v \sin i$ value of the close visual companion is 4 km s^{-1}. Such a low value is consistent with that component being a late-F or early-G dwarf. Such stars are usually expected to be rotating slowly because of angular momentum loss.

7.4. 18 Vul

The 18 Vul system also has a slight eccentricity of 0.01, but again this value is so small that there is little difference between the synchronous and pseudosynchronous periods, and so we simply adopt the orbital period and discuss the possibility of synchronous rotation for the components of this system. The projected rotational velocities of both stars are at least four to five times greater than those of the other stars in this work, as we obtain 42 ± 2 and 51 ± 3 km s^{-1} for the primary and secondary,

respectively. With the radii from the Stefan–Boltzmann law, the synchronous velocities for the two components are 19.0 and 13.0 km s^{-1}. In Figure 13, the position of the primary in the H-R diagram indicates a mass of 2.4 $M_\odot$. That value, combined with its $m \sin^3 i$, results in an orbital inclination of 72°. Adopting that inclination, the equatorial rotational velocities become 44.2 and 53.6 km s^{-1} for the primary and secondary, respectively. Both values are substantially larger than the computed synchronous ones, so neither component is close to synchronous rotation. The observed and predicted rotational velocities are compared in Table 11.

8. CONCLUSIONS

We have determined improved orbital elements for four double-lined spectroscopic binaries, HR 1528, HR 6993, 2 Sge, and 18 Vul. The three systems with periods less than 10 days have circular or nearly circular orbits. Only HR 6933 with a period of 14.68 days has a moderate eccentricity. The very faint, close visual component of the 2 Sge short-period binary, which was discovered by the *Hipparcos* team (Perryman et al. 1997), is detected spectroscopically at red wavelengths. The minimum masses of the eight short-period binary components have been determined to an accuracy of 0.5% or better. Four of the eight components may be rotating synchronously or pseudosynchronously.

From the reanalyzed *Hipparcos* parallaxes (van Leeuwen 2007) and adopted masses of the systems, we estimate either the maximum angular separations of the components or in the case of the eccentric system HR 6993, the maximum angular nodal separation of the components (e.g., McAlister 1976; Halbwachs 1981). Similar to the results of Halbwachs (1981), we find that the separations all are in the 1–2 mas range, and therefore, although quite small, are still within the scope of modern optical interferometers. Thus, when our spectroscopic results are complemented with high-quality interferometric results, accurate three-dimensional orbits, masses, and distances for the systems will follow, allowing improved comparisons with evolutionary tracks.

REFERENCES

Abt, H. A., & Bidelman, W. P. 1969, ApJ, 158, 1091
Abt, H. A., & Morrell, N. I. 1995, ApJS, 99, 135
Abt, H. A., & Moyd, K. I. 1973, ApJ, 182, 809
Adams, W. S. 1912, ApJ, 35, 163
Adams, W. S. 1915, ApJ, 42, 172

Appenzeller, I. 1967, PASP, 79, 102
Barden, S. C. 1985, ApJ, 295, 162
Barker, E. S., Evans, D. S., & Laing, J. D. 1967, RGOB, 130, 355
Batten, A. H., Fletcher, J. M., & MacCarthy, D. G. 1989, PDAO, 17, 1
Belmonte, J. A., & Roca Cortés, T. 1989, IBVS, 3344, 1
Bertaud, C. 1970, A&AS, 1, 7
Bertaud, C., & Floquet, M. 1967, JO, 50, 425
Boden, A. F., Torres, G., & Latham, D. W. 2006, ApJ, 644, 1193
Breger, M. 1969, ApJS, 19, 79
Cowley, A. P., Cowley, C. R., Jaschek, M., & Jaschek, C. 1969, AJ, 74, 375
Crawford, D. L. 1979, AJ, 84, 1858
Cucchiaro, A., Macau-Hercot, D., Jaschek, M., & Jaschek, C. 1978, A&AS, 33, 15
Cunha, M. S. 2007, A&ARv, 14, 217
Eaton, J. A., & Williamson, M. H. 2004, Proc. SPIE, 5496, 710
Eaton, J. A., & Williamson, M. H. 2007, PASP, 119, 886
Fabricius, C., & Makarov, V. V. 2000, A&A, 356, 141
Fekel, F. C. 1997, PASP, 109, 514
Fekel, F. C. 1999, in ASP Conf. Ser. 185, IAU Colloquium 170, Precise Stellar Radial Velocities, ed. J. B. Hearnshaw & C. D. Scarfe (San Francisco, CA: ASP), 378
Fekel, F. C., Boden, A. F., Tomkin, J., & Torres, G. 2009a, ApJ, 695, 1527
Fekel, F. C., Rajabi, S., Muterspaugh, M. W., & Williamson, M. H. 2013, AJ, 145, 111
Fekel, F. C., Tomkin, J., & Williamson, M. H. 2009b, AJ, 137, 3900
Fekel, F. C., Tomkin, J., & Williamson, M. H. 2010, AJ, 139, 1579
Fekel, F. C., Tomkin, J., Williamson, M. H., & Pourbaix, D. 2011a, AJ, 142, 69
Fekel, F. C., & Williamson, M. H. 2010, AJ, 140, 1381
Fekel, F. C., Williamson, M. H., & Henry, G. W. 2011b, AJ, 141, 145
Floquet, M. 1975, A&AS, 21, 25
Flower, P. J. 1996, ApJ, 469, 355
Geary, J. C., & Abt, H. A. 1970, AJ, 75, 718
Girardi, L., Bressan, A., Bertelli, G., & Chiosi, C. 2000, A&AS, 141, 371
Gray, D. F. 1992, The Observation and Analysis of Stellar Photospheres (Cambridge: Cambridge Univ. Press)
Halbwachs, J. L. 1981, A&AS, 44, 47
Harper, W. E. 1918, JRASC, 12, 392
Harper, W. E. 1932a, PDAO, 6, 79
Harper, W. E. 1932b, PDAO, 7, 1
Harper, W. E. 1935, PDAO, 6, 207
Huenemoerder, D. P., & Barden, S. C. 1984, BAAS, 16, 510
Hummel, C. A., Carquillat, J.-M., Ginestet, N., et al. 2001, AJ, 121, 1623

Hut, P. 1981, A&A, 99, 126
Johnson, H. L. 1966, ARA&A, 4, 193
Lacy, C. H. S., & Fekel, F. C. 2011, AJ, 142, 185
Levato, H. 1975, A&AS, 19, 91
Levato, H., & Abt, H. A. 1978, PASP, 90, 429
Lucy, L. B., & Sweeney, M. A. 1971, AJ, 76, 544
Luyten, W. J. 1936, ApJ, 84, 85
Mason, B. D., Martin, C., Hartkopf, W. I., et al. 1999, AJ, 117, 1890
Matthews, L. D., & Mathieu, R. D. 1992, in ASP Conf. Ser. 32, IAU Colloquium 135, Complimentary Approaches to Double and Multiple Star Research, ed. H. A. McAlister & W. I. Hartkopf (San Francisco, CA: ASP), 244
McAlister, H. A. 1976, PASP, 88, 317
McAlister, H. A., Hartkopf, W. I., Hutter, D. J., & Franz, O. G. 1987, AJ, 93, 688
McCarthy, J. A., Sandiford, B. A., Boyd, D., & Booth, J. 1993, PASP, 105, 881
Osawa, K. 1959, ApJ, 130, 159
Perryman, M. A. C., Lindegren, L., Kovalevsky, J., et al. 1997, A&A, 323, L49
Petrie, R. M. 1948, PDAO, 7, 415
Petrie, R. M. 1950, PDAO, 8, 319
Pintado, O. I., & Adelman, S. J. 2003, A&A, 406, 987
Pourbaix, D., Tokovinin, A. A., Batten, A. H., et al. 2004, A&A, 424, 727
Quirrenbach, A. 2001, ARA&A, 39, 353
Roberts, L. C. 2011, MNRAS, 413, 1200
Rodríguez, E., López de Coca, P., Rolland, A., Garrido, R., & Costa, V. 1994, A&AS, 106, 21
Scarfe, C. D., Batten, A. H., & Fletcher, J. M. 1990, PDAO, 18, 21
Stickland, D. J. 1973, MNRAS, 161, 193
Stockton, R. A., & Fekel, F. C. 1992, MNRAS, 256, 575
Stokes, N. R. 1972, MNRAS, 160, 155
Strassmeier, K. G., & Fekel, F. C. 1990, A&A, 230, 389
Svolopoulos, S. N. 1961, ApJ, 134, 612
Tassoul, J.-L., & Tassoul, M. 1992, ApJ, 395, 259
Tomkin, J., & Fekel, F. C. 2006, AJ, 131, 2652
Tomkin, J., & Fekel, F. C. 2008, AJ, 135, 555
Torres, G., Andersen, J., & Giménez, A. 2010, A&ARv, 18, 67
van Leeuwen, F. 2007, Hipparcos, The New Reduction of the Raw Data (Dordrecht: Springer)
Wolfe, R. H., Horak, H. G., & Storer, N. W. 1967, in Modern Astrophysics, ed. M. Hack (New York: Gordon & Breach), 251
Young, R. K. 1917, JRASC, 11, 127
Zahn, J.-P. 1977, A&A, 57, 383